A PHYSICALLY-BASED SCHEME FOR THE URBAN ENERGY BUDGET IN ATMOSPHERIC MODELS

VALÉRY MASSON*
Centre National de Recherches Météorologiques, Toulouse, France

(Received in final form 29 September 1999)

Abstract. An urban surface scheme for atmospheric mesoscale models is presented. A generalization of local canyon geometry is defined instead of the usual bare soil formulation currently used to represent cities in atmospheric models. This allows refinement of the radiative budgets as well as momentum, turbulent heat and ground fluxes. The scheme is aimed to be as general as possible, in order to represent any city in the world, for any time or weather condition (heat island cooling by night, urban wake, water evaporation after rainfall and snow effects).

Two main parts of the scheme are validated against published data. Firstly, it is shown that the evolution of the model-predicted fluxes during a night with calm winds is satisfactory, considering both the longwave budget and the surface temperatures. Secondly, the original shortwave scheme is tested off-line and compared to the effective albedo of a canyon scale model. These two validations show that the radiative energy input to the urban surface model is realistic.

Sensitivity tests of the model are performed for one-year simulation periods, for both oceanic and continental climates. The scheme has the ability to retrieve, without ad hoc assumptions, the diurnal hysteresis between the turbulent heat flux and ground heat flux. It reproduces the damping of the daytime turbulent heat flux by the heat storage flux observed in city centres. The latent heat flux is negligible on average, but can be large when short time scales are considered (especially after rainfall). It also suggests that in densely built areas, domestic heating can overwhelm the net radiation, and supply a continuous turbulent heat flux towards the atmosphere. This becomes very important in winter for continental climates. Finally, a comparison with a vegetation scheme shows that the suburban environment can be represented with a bare soil formulation for large temporal or spatial averages (typical of global climatic studies), but that a surface scheme dedicated to the urban surface is necessary when smaller scales are considered: town meteorological forecasts, mesoscale or local studies.

Keywords: Surface scheme, Urban Canyon, Urban energy balance, Urban water balance, Urban boundary layer.

1. Introduction

Due to the complexity and diversity of towns around the world, conclusions drawn from experimental studies on the interaction between the atmosphere and urbanized areas most of the time are limited either to a particular site or physical processes. To overcome this problem, numerical studies are aimed to simulate the urban climatology or energy budget. However, they still follow rather simplified

* E-mail: valery.masson@meteo.fr

Boundary-Layer Meteorology **94:** 357–397, 2000.

approaches. Building-resolving models, i.e., models in which individual building shapes are described, allow the detailed examination of specific processes (radiative effects, see for for example, Terjung and O'Rourke (1980), or wind channeling), but because of computational cost, applications are limited to local urbanization and comfort studies. Simpler building-averaged models have also been developed. The most famous is the 'canyon' model, from Oke and colleagues developed during the seventies, dedicated to urban streets, where a road is bordered by two facing building walls. Several numerical models have been developed using the canyon geometry (Johnson et al., 1991; Mills, 1993; Arnfield et al., 1998) to study radiative trapping, surface energy budgets (using multiple facets for each surface) or canyon winds.

The two model types presented above are used in urban climatology in order to comprehend town energetics. The next modelling step is to perform a coupling between the urban surface and the atmosphere in mesoscale atmospheric models. The most common way to do this is to use a vegetation-atmosphere transfer model, whose parameters have been modified (Seaman et al., 1989; Menut, 1997), as opposed to an urban model. Cities are then modelled as bare soil or as a concrete plate. The roughness length is often large (one to a few metres, see Wieringa, 1993; or Petersen, 1997). The soil moisture availability (or the soil depth) is reduced, so that the Bowen ratio is shifted towards high values (viz. large sensible heat flux). The most recent works tend to simulate other factors, such as heat storage, by the use of a concrete canopy above the surface. A horizontal plate is in radiative interaction with the surface in Best (1998), and the treatment is similar to a forest canopy in Soux et al. (1998). The Taha (1999) mesoscale study uses a semi-empirical formulation for the heat storage flux – the Objective Hysteresis Model by Grimmond et al. (1991).

The above illustrates the gap between the state of the art in urban climatology and its parameterization in atmospheric models. The objective of the present paper is to present an urban model that links the climatologists' approach of city representation to an atmospheric model.

The Town Energy Budget (TEB) scheme is built following the canyon approach, generalized in order to represent larger horizontal scales. The physics treated by the scheme are relatively complete. Due to the complex shape of the city surface, the urban energy budget is split into different parts: *three* surface energy budgets are considered: one for the roofs, roads, and walls. Orientation effects are averaged for roads and walls. Up to two energy budgets are added for snow when this is present on roofs or roads. Some of the physics were derived from the literature (longwave radiation or thermal conduction through the surfaces), since they are classically assumed to estimate temperatures in conditions without feedback towards the atmosphere (during nights with calm wind). However, most parts of the physics need an original approach (shortwave radiation, thermodynamical and anthropogenic flux treatment, rain and snow), since they occur when interaction with the atmosphere is strong.

The TEB scheme is presented in Section 2. A validation of some aspects of the scheme is shown in Section 3, and sensitivity experiments using single-year atmospheric forcings are discussed in Section 4. Conclusions are given in Section 5.

2. Presentation of the Town Energy Budget Scheme

2.1. OBJECTIVES

The TEB model is aimed to simulate the turbulent fluxes into the atmosphere at the surface of a mesoscale atmospheric model covered by buildings, roads, or any artificial material. It should parameterize both the urban surface and the roughness sublayer, so that the atmospheric model only 'sees' a constant flux layer as its lower boundary.

The TEB scheme must be considered as part of the surface parameterization of the atmospheric model. The fluxes should be computed for each land type by the appropriate scheme, and then averaged in the atmospheric model grid mesh, with respect to the proportion occupied by each type. For example, partitions should be: (1) sea; (2) inland water; (3) natural and cultivated terrestrial surface; (4) towns. The following fluxes are calculated: latent and sensible heat fluxes (W m^{-2}), upward radiative fluxes (W m^{-2}) and component momentum fluxes (m^2 s^{-2}).

2.2. TOWN GEOMETRY DESCRIPTION

Numerous fine-scale studies on building climatology exist. In these, several individual buildings are usually present in order to study their radiative interaction, the wind channeling effects, or the building insulation characteristics. The *canyon* concept, developed by city climatologists (e.g., Oke, 1987), uses such a framework: it considers a single road, bordered by facing buildings. In these studies, models are, at best, forced by atmospheric data (radiation, wind above the roofs) but are not interactive with it.

The TEB model aims to parameterize town-atmosphere dynamic and thermodynamic interactions. It is applicable for mesoscale atmospheric models (a grid mesh larger than a few hundred metres). Then, spatial averaging of the town characteristics, as well as its effect on the atmosphere, are necessary. The individual shapes of each building are no longer taken into account, so that TEB geometry is based on the canyon hypothesis. However, a single canyon would be too restrictive at the considered horizontal scale.

We therefore use the following original city representation:

1. The buildings have the same height and width (in the model mesh), with the roof level at the surface level of the atmospheric model.

TABLE I

Parameters of the TEB scheme. Note that a_{town} is not strictly a parameter of the TEB scheme, but is used to average the output TEB fluxes with those computed for the vegetation and water portions of the grid mesh. Note also that some surfaces between the buildings, such as gardens or parks, for example, are *not* treated by the TEB model, but modify the canyon width, w.

Symbol	Designation of symbol	Unit
Geometric parameters		
a_{town}	Fractional area occupied by artificial material	–
a_{bld}	Fractional artificial area occupied by buildings	–
$1 - a_{\text{bld}}$	Fractional artificial area occupied by roads	–
h	Building height	m
h/l	Building aspect ratio	–
h/w	Canyon aspect ratio	–
$z0_{\text{town}}$	Dynamic roughness length for the building/canyon system	m
Radiative parameters		
$\alpha_R, \alpha_r, \alpha_w$	Roof, road and wall albedos	–
$\epsilon_R, \epsilon_r, \epsilon_w$	Roof, road and wall emissivities	–
Thermal parameters		
$d_{R_k}, d_{r_k}, d_{w_k}$	Thickness of the kth roof, road or wall layer	m
$\lambda_{R_k}, \lambda_{r_k}, \lambda_{w_k}$	Thermal conductivity of the kth roof, road or wall layer	W m^{-1} K^{-1}
$C_{R_k}, C_{r_k}, C_{w_k}$	Heat capacity of the kth roof, road or wall layer	J m^{-3} K^{-1}

2. Buildings are located along identical roads, the length of which is considered far greater than their width; the space contained between two facing buildings is defined as a canyon.
3. Any road orientation is possible, and all exist with the same probability. This hypothesis allows the computation of averaged forcing for road and wall surfaces. In other words, when the canyon orientation appears in a formula (with respect to the sun or the wind direction), it is averaged over 360°. In this way, no discretization is performed on the orientation.

These hypotheses, as well as the formulations chosen for the physics (see hereafter), allow the development of a relatively simple scheme. The parameters describing the city are displayed in Table I, and the scheme variables can be found in Table II.

The TEB model does not use one urban surface temperature (representative of the entire urban cover), but *three* surface temperatures, representative of roofs, roads and walls. There are two reasons for this:

– Urban climatologists generally consider complex (non-flat) geometry cases, in particular the ‘canyon’ geometry. In order to be consistent with their findings,

TABLE II
Energy fluxes and variables in the TEB scheme.

Symbol	Designation of symbol	Unit
Prognostic variables		
T_{R_k}, T_{r_k}, T_{w_k}	Temperature of the kth roof, road or wall layer	K
W_R, W_r	Roof and road water interception reservoir	kg m^{-2}
W_{snow_R}, W_{snow_r}	Roof and road snow interception reservoir	kg m^{-2}
T_{snow_R}, T_{snow_r}	Roof and road snow temperature	K
ρ_{snow_R}, ρ_{snow_r}	Roof and road snow density	kg m^{-3}
α_{snow_R}, α_{snow_r}	Roof and road snow albedo	–
Diagnostic variables		
T_{can}	Canyon air temperature	K
q_{can}	Canyon air specific humidity	kg kg^{-1}
U_{can}	Along canyon horizontal wind	m s^{-1}
α_{town}	Town effective albedo	–
T_{town}	Town area averaged radiative surface temperature	K
Input energy fluxes		
$L^{\downarrow}$	Downward infrared radiation on an horizontal surface	W m^{-2}
$S^{\downarrow}$	Downward *diffuse* solar radiation on an horizontal surface	W m^{-2}
$S^{\Downarrow}$	Downward *direct* solar radiation on an horizontal surface	W m^{-2}
H_{traffic}	Anthropogenic sensible heat flux released in the canyon	W m^{-2}
LE_{traffic}	Anthropogenic latent heat flux released in the canyon	W m^{-2}
H_{industry}	Anthropogenic sensible heat flux released by industries	W m^{-2}
LE_{industry}	Anthropogenic latent heat flux released by industries	W m^{-2}
Other energy input		
$T_{i_{\text{bld}}}$	Building interior temperature	K
Output energy fluxes		
S_R^*, S_r^*, S_w^*	Net solar radiation budget for roofs, roads and walls	W m^{-2}
L_R^*, L_r^*, L_w^*	Net infra-red radiation budget for roofs, roads and walls	W m^{-2}
H_R, H_r, H_w	Turbulent sensible heat flux for roofs, roads and walls	W m^{-2}
LE_R, LE_r, LE_w	Turbulent latent heat flux for roofs, roads and walls	W m^{-2}
$G_{R_{k,k+1}}$, $G_{r_{k,k+1}}$, $G_{w_{k,k+1}}$	Conduction heat flux between kth and $k+1$th roof, road or wall layers	W m^{-2}
H_{town}	Town averaged turbulent sensible heat flux	W m^{-2}
LE_{town}	Town averaged turbulent latent heat flux	W m^{-2}

the TEB model uses a complex surface consisting of multiple explicit energy budgets.

– One spatially-averaged surface temperature is often used in soil-vegetation schemes, in order to compute the turbulent fluxes towards the atmosphere according to Monin–Obukhov similarity theory. However, over towns, the use of only one temperature should be debatable, because it is observed that the Monin–Obukhov similarity theory does not apply for temperature in the urban roughness sublayer.

The second point will be addressed in more detail in Section 2.9. The parameters of the scheme depend directly on building shapes and construction materials. This makes the TEB scheme easy to initialize, without the need for any atmospheric data for parameter tuning. Construction material characteristics can be found in the literature (e.g., see Oke, 1988).

One must separately treat roads and walls, as they occur differently in all the physical processes under consideration (sky viewing, thermal structure, source of heating inside the buildings, or the presence of water or snow on the road). In contrast, the sunlit and shadowed walls are not treated separately, as the two facing walls are identical for all processes, except one, the direct solar radiation. Note that the two walls behave similarly for the scattered solar radiation (i.e., in cloudy conditions). The problem here is that it is not clear how to separate sunlit and shadowed walls. The situation would be relatively straightforward if there was only one street direction, but at the town scale, this is not so, and streets parallel or perpendicular to the sun direction are found. To treat separately the walls, according to illumination by the sun, would necessitate a separate treatment for the street directions. A discretization for the streets should be performed at least every 45 or 30°, leading respectively to four or six energy budgets for roads, and twice as many for walls. Furthermore, the effect of the longwave radiation non-linearities produced by a single wall temperature is very small. Supposing a canyon with a road width equal to the building height (leading to a sky-view factor for the walls of $\Psi_w = 0.3$, see Section 2.6) and a wall emissivity of 0.85, the difference in the canyon-top budget between two walls at 290 K, or two walls at 280 and 300 K, is only 1.5 W m^{-2}. Therefore, for sake of scheme simplicity, only one energy budget is chosen for the walls. Particular attention is still paid to the solar radiation budget, and the validation presented in Section 3.2 shows it is accurate at canyon scale.

2.3. TEMPERATURE EVOLUTION EQUATIONS

As discussed above, the urban surface is very inhomogeneous with respect to shape and building materials. Urban climatologists need at least four component surfaces to describe it: the roof, the road, and two facing walls. The problem considered here (the evaluation of the turbulent and radiative fluxes from the urban cover to the atmosphere) allows the treatment of only three types of surfaces (roof, road, wall), while keeping enough accuracy to correctly represent the different terms of the

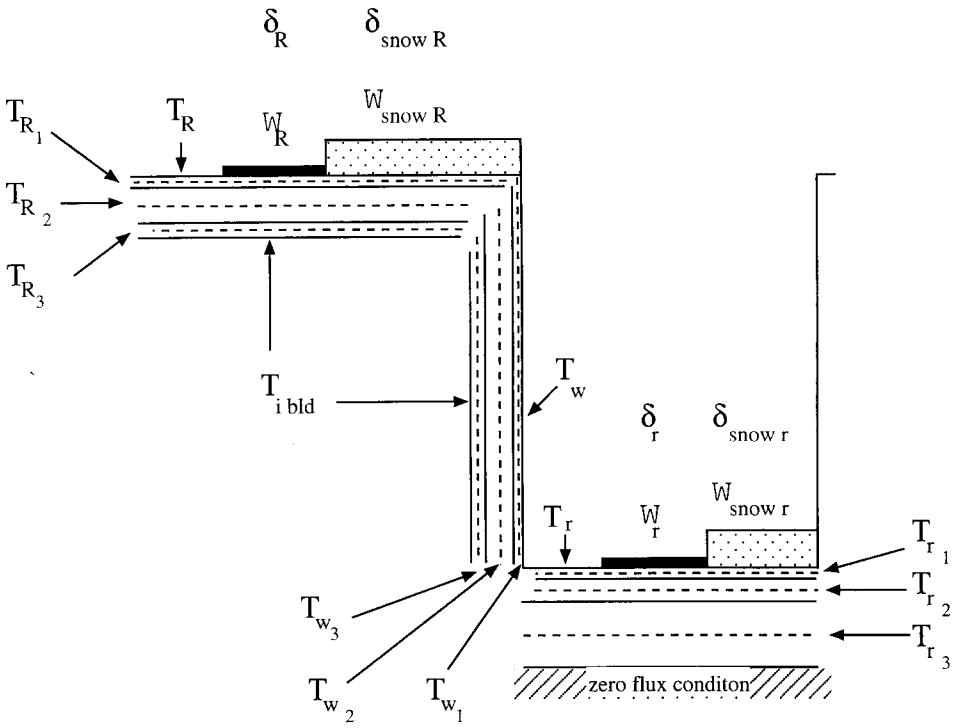

Figure 1. Discretization of the surfaces (roof, wall, road) and prognostic variables: layer temperatures $T_{\star_k}$ ($\star = R, w, r$; here three layers are displayed for each surface, so $k = 1, 2, 3$), surface water content $W_\star$ ($\star = R, r$), surface snow content $W_{\text{snow}_\star}$ ($\star = R, r$). The layer temperatures are representative of the middle of each layer (dotted lines). The surface temperatures are assumed to be equal to the surface-layer temperature: $T_\star = T_{\star_k}$. The internal building temperature $T_{i_{\text{bld}}}$ is prescribed. Fractions of water or snow ($\delta_\star$ and $\delta_{\text{snow}_\star}$ respectively) are computed from the water and snow contents (see text). Snow density, albedo and temperature are computed independently for roof and road by a snow mantel scheme (in this paper, a one-layer scheme was chosen).

surface energy budget. This is why the TEB model uses *three* surface temperatures, T_R, T_r and T_w, representative of roofs, roads and walls, respectively.

Furthermore, in order to treat the conduction fluxes to or from the building interiors (roof, wall) or the ground (road), each surface type is discretized into several layers (Figure 1). By convention, the layer with subscript 1 is the one in contact with the air (hereafter ‘surface layer’).

The equations describing the evolution of the temperatures of the layers (representative of the middle of each layer) are based on energy budget considerations. The prognostic equations for the surface layers of the roof, wall and road respectively, read:

$$C_{R_1}\frac{\partial T_{R_1}}{\partial t} = (1-\delta_{\text{snow}_R})\frac{1}{d_{R_1}}\left(S^*_R + L^*_R - H_R - LE_R - G_{R_{1,2}}\right) + \delta_{\text{snow}_R}\frac{1}{d_{R_1}}\left(G_{R_{\text{snow},1}} - G_{R_{1,2}}\right) \quad (1a)$$

$$C_{w_1}\frac{\partial T_{w_1}}{\partial t} = \frac{1}{d_{w_1}}\left(S^*_w + L^*_w - H_w - G_{w_{1,2}}\right) \quad (1b)$$

$$C_{r_1}\frac{\partial T_{r_1}}{\partial t} = (1-\delta_{\text{snow}_r})\frac{1}{d_{r_1}}\left(S^*_r + L^*_r - H_r - LE_r - G_{r_{1,2}}\right) + \delta_{\text{snow}_r}\frac{1}{d_{r_1}}\left(G_{r_{\text{snow},1}} - G_{r_{1,2}}\right). \quad (1c)$$

These three equations can be written in a generic way:

$$C_{\star_1}\frac{\partial T_{\star_1}}{\partial t} = (1-\delta_{\text{snow}_\star})\frac{1}{d_{\star_1}}\left(S^*_\star + L^*_\star - H_\star - LE_\star - G_{\star_{1,2}}\right) + \delta_{\text{snow}_\star}\frac{1}{d_{\star_1}}\left(G_{\star_{\text{snow},1}} - G_{\star_{1,2}}\right), \quad (1d)$$

where, the subscript $\star$ denotes either R, r or w, describing roof, road and wall variables (only the roof and road for water variables) respectively. This convention is used in the rest of the paper. Here, $T_{\star_k}$ is the temperature of the kth layer of the considered surface (in the above equations, $k = 1$); $C_{\star_k}$ represents the heat capacity, λ_k the thermal conductivity and $d_{\star_k}$ the layer thickness.

The fluxes $S^*_\star$, $L^*_\star$, $H_\star$, $LE_\star$, $G_{\star_{1,2}}$ and $G_{\star_{\text{snow},1}}$ denotes net solar radiation, net infrared radiation, sensible heat flux, latent heat flux, and conduction heat flux between the surface layer and the underlying layer, conduction heat fluxes between the base of the snow mantel and the surface, respectively; $\delta_{\text{snow}_\star}$ is the snow fraction on the surface (which is zero on the walls).

It is assumed that the surface layer of each surface is sufficiently thin such that the layer-averaged temperature can be used to evaluate the radiative and turbulent surface fluxes. This means that the surface temperatures $T_\star$ are computed as:

$$T_\star = T_{\star_1}.$$

For the sake of clarity, the 1 subscript will be removed in the following sections.

The other layer temperatures evolve according to a simple heat conduction equation. For the kth layer:

$$C_{\star_k}\frac{\partial T_{\star_k}}{\partial t} = \frac{1}{d_{\star_k}}\left(G_{\star_{k-1,k}} - G_{\star_{k,k+1}}\right). \quad (2)$$

In these equations, the conduction flux between layers k and $k+1$ reads (for $k < n$ where n is the number of layers):

$$G_{\star_{k,k+1}} = \overline{\lambda}_{k,k+1} \frac{T_{\star_k} - T_{\star_{k+1}}}{\frac{1}{2}(d_{\star_k} + d_{\star_{k+1}})} \tag{3}$$

with

$$\overline{\lambda}_{k,k+1} = \frac{d_{\star_k} + d_{\star_{k+1}}}{(d_{\star_k}/\lambda_k) + (d_{\star_{k+1}}/\lambda_{k+1})}. \tag{4}$$

The lower boundary conditions for the roofs and walls are given by the building internal temperature, that for the road being represented as a zero flux lower boundary. The fluxes between the nth layer (the inner layer) and the underlying material are then:

$$G_{R_{n,n+1}} = \lambda_n \frac{T_{R_n} - T_{i_{bld}}}{\frac{1}{2}(d_{R_n})}, \tag{5}$$

$$G_{w_{n,n+1}} = \lambda_n \frac{T_{w_n} - T_{i_{bld}}}{\frac{1}{2}(d_{w_n})}, \tag{6}$$

$$G_{r_{n,n+1}} = 0. \tag{7}$$

Note that the number of layers for roof, wall and road can differ. In this study, three layers for each surface are chosen. Due to large temperature gradients that can exist, and because of the multi-layer structure of the walls or the roofs, it is recommended that at least three layers are used to represent each surface.

2.4. WATER RESERVOIR EVOLUTION

Liquid or solid precipitation intercepted by urban surfaces is rarely addressed in the literature, except for sewer system and hydrological considerations. An exception is Grimmond and Oke (1991), however, in which the model used was initially dedicated to forest studies, and is limited to the water budget computed from the Penman–Monteith equation. They added anthropogenic water sources and used the Grimmond et al. (1991) heat storage flux formulation.

Because of the presence of the surface temperatures in the TEB scheme, the saturation specific humidity, and thus the turbulent latent heat flux, can be computed more easily (see Section 2.9). The liquid precipitation is intercepted by both roofs and roads, and there is runoff from roofs and roads to the sewer system. Roads and roofs can be covered by a certain amount of water, parameterized by the variables W_r and W_R, respectively. These surfaces are impervious. Then, instead of defining a relative humidity, it is more judicious to treat the fraction of surface covered by

the water, δ_r and δ_R. This part is saturated (fractional water pools), while the other part is assumed to be dry. Water evaporates when the air humidity is unsaturated until all water has disappeared from the impervious surface.

The snow-free fraction of the surface occupied by liquid water is computed as $\delta_\star = (W_\star / W_{\star_{\max}})^{\frac{2}{3}}$ (Noilhan and Planton, 1989), where $W_{\star_{\max}}$ is the maximum water amount on the surface.

Furthermore, urban dew is taken into account (in the case of negative latent heat flux), as its occurrence can have significant effects, as pointed out by Richards and Oke (1998). It requires a special treatment: when conditions are present for dew to occur (air humidity larger than the surface saturation humidity), the surface is considered wet ($\delta_* = 1$). This allows then a negative latent heat flux, and hence dewfall that can fill the interception reservoirs. These treatments are deduced from those for the foliage interception reservoirs in vegetation schemes (Deardorff, 1978; Noilhan and Planton, 1989).

Addition of an anthropogenic water source was not retained in TEB, because it does not compute evaporation from gardens or parks. Irrigation water input should be taken into account through the vegetation scheme dedicated to these natural surfaces. However, anthropogenic fluxes of water vapour directly into the air exist in the scheme (see Section 2.9), in order to represent factory release, for example.

Finally, the water-reservoir evolution equation is (for roof or road):

$$\frac{\partial W_\star}{\partial t} = R - LE_\star / L_v, \quad (W_\star < W_{\star_{\max}}), \tag{8}$$

where R is the rain rate (kg m^{-2} s^{-1}) and L_v is the latent heat of vaporization.

The reservoirs are of small capacity, and the water in excess is lost as runoff. They are set equal to $W_{R_{\max}} = W_{r_{\max}} = 1$ kg m^{-2}, which is well in the range of values explored by Grimmond and Oke (1991). The total depletion of the reservoirs by evaporation requires, in general, a few hours of daytime conditions.

2.5. SNOW EFFECTS

Snow is intercepted by roofs and roads, and a snow scheme is implemented on each surface type. Snow density, albedo, temperature and thickness of water equivalent depth are parameterized, and radiation, sensible heat flux, sublimation, conduction and melting are taken into account.

The evolution rate of the snow albedo is enhanced (and its minimum value lowered) in order to represent car pollution (dirty snow). A time-dependent drainage term is included to take into account snow-plow work (if any).

The snow fraction on roof or road surfaces is set equal to a function of the snow interception reservoir ($W_{\text{snow}\star}$): $\delta_{\text{snow}\star} = W_{\text{snow}\star}/(W_{\text{snow}\star} + W_{\text{snow}\star_{\max}})$. The parameter $W_{\text{snow}\star_{\max}}$ is set equal to 1 kg m^{-2}. The snow has an effect on:

– the energy budget of the surfaces (since part of the downward heat flux arises from the base of the snow),

– the heat fluxes from the road towards the canyon or from the roof towards the atmosphere,
– the radiative calculations for the canyon surfaces, because of the snow albedo, emissivity and temperature.

2.6. LONGWAVE BUDGET

The trapping of longwave radiation by the canyon surfaces is computed with one re-emission taken into account (from the Johnson et al. (1991) formulation).

The sky-view factors are needed, and are computed for the TEB geometry (an infinite canyon) according to Noilhan (1981):

$$\Psi_r = [(h/w)^2 + 1]^{1/2} - h/w, \tag{9}$$

$$\Psi_w = \frac{1}{2}\{h/w + 1 - [(h/w)^2 + 1]^{1/2}\}/(h/w). \tag{10}$$

These factors represent the fraction of sky seen from the road and one wall respectively, compared to the sky fraction that a flat horizontal surface would see without obstruction. The sky-factor for the roof is then equal to 1. If the buildings are very low, Ψ_r tends to 1 and Ψ_w to 0.5 (one wall then sees one half of the sky). In this case, longwave radiative fluxes from the roads will be unperturbed by the walls. On the contrary, if the buildings are very tall, both sky factors tend to zero, and radiative exchanges will mostly occur between the walls, and less energy will escape towards the sky.

The net longwave radiation absorbed by the snow-free road and wall surfaces is given as:

$$\begin{aligned} L_r^* \;=\; & \epsilon_r \Psi_r L^{\downarrow} - \epsilon_r \sigma T_r^4 + \epsilon_r \epsilon_w (1 - \Psi_r) \sigma T_w^4 \\ & + \epsilon_r (1 - \epsilon_w)(1 - \Psi_r) \Psi_w L^{\downarrow} + \epsilon_r \epsilon_w (1 - \epsilon_w)(1 - \Psi_r)(1 - 2\Psi_w) \sigma T_w^4 \\ & + \epsilon_r (1 - \epsilon_w)(1 - \Psi_r) \Psi_w \sigma \overline{\epsilon_r T_r^4}, \end{aligned} \tag{11}$$

$$\begin{aligned} L_w^* \;=\; & \epsilon_w \Psi_w L^{\downarrow} - \epsilon_w \sigma T_w^4 + \epsilon_w \Psi_w \sigma \overline{\epsilon_r T_r^4} \\ & + \epsilon_w^2 (1 - 2\Psi_w) \sigma T_w^4 + \epsilon_w (1 - \overline{\epsilon_r}) \Psi_w \Psi_r L^{\downarrow} \\ & + \epsilon_w (1 - \epsilon_w) \Psi_w (1 - 2\Psi_w) L^{\downarrow} + \epsilon_w^2 (1 - \epsilon_w)(1 - 2\Psi_w)^2 \sigma T_w^4 \\ & + \epsilon_w^2 (1 - \overline{\epsilon_r}) \Psi_w (1 - \Psi_r) \sigma T_w^4 + \epsilon_w (1 - \epsilon_w) \Psi_w (1 - 2\Psi_w) \sigma \overline{\epsilon_r T_r^4}, \end{aligned} \tag{12}$$

where

$$\overline{\epsilon_r} = (1 - \delta_{\mathrm{snow}_r})\epsilon_r + \delta_{\mathrm{snow}_r} \epsilon_{r_{\mathrm{snow}}},$$

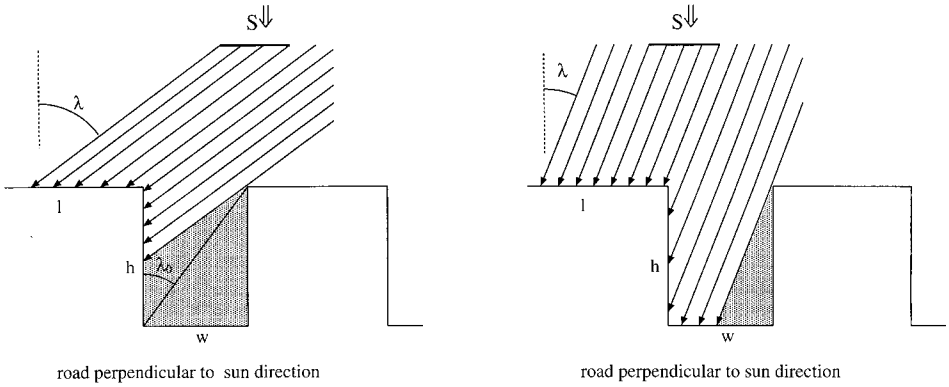

Figure 2. Solar radiation received in a canyon perpendicular to the sun direction; left hand: sun low over the horizon ($\lambda > \lambda_0$); right hand: sun high over the horizon ($\lambda < \lambda_0$).

$$\overline{\epsilon_r T_r^4} = (1 - \delta_{\text{snow}_r})\epsilon_r T_r^4 + \delta_{\text{snow}_r}\epsilon_{r_{\text{snow}}} T_{\text{snow}_r}^4 .$$

By inverting the snow-covered and snow-free road characteristics in Equation (11), the longwave radiative budget on the top of the snow mantel can be defined. To deduce Equations (11) and (12), we used the fact that, if Ψ_r represents the contribution of the sky to the road viewing, then $(1 - \Psi_r)$ is the contribution of the two walls. For the budget of one wall, the sky-view factor is Ψ_w, the road-view factor is Ψ_w (per symmetry), and the facing wall-view factor is $(1 - 2\Psi_w)$.

2.7. SOLAR RADIATION

2.7.1. *Direct Solar Radiation*

Because of shadow effects, special computations are required to estimate the solar flux received either by the walls or the roads.

Let $S^{\Downarrow}$ be the direct solar radiation received by a *horizontal* surface at the first atmospheric model level; the roof surface receives this amount of radiation. Let θ be the angle between the sun direction and the canyon axis, and λ be the solar zenith angle (from zenith). Let us first consider a road perpendicular to the sun's direction ($\theta = \pi/2$, Figure 2); $\lambda_0 = \arctan(w/h)$ is defined as the zenith angle for which the sun begins to illuminate the road. It can be noted that, whatever the sun position, one of the two walls is in shadow, the other one is partially in light.

The mean direct solar fluxes received by both walls and by the road, for a street direction perpendicular to the sun, are:

$$S_w^{\Downarrow}\left(\theta = \frac{\pi}{2}\right) = \begin{cases} \dfrac{1}{2}\dfrac{w}{h} S^{\Downarrow} & \text{if } \lambda > \lambda_0 \\ \dfrac{1}{2}\tan(\lambda) S^{\Downarrow} & \text{if } \lambda < \lambda_0, \end{cases}$$

$$S_r^{\Downarrow}\left(\theta=\frac{\pi}{2}\right)=\begin{cases}0 & \text{if } \lambda>\lambda_0\\ \left(1-\dfrac{h}{w}\tan(\lambda)\right)S^{\Downarrow} & \text{if } \lambda<\lambda_0.\end{cases}$$

In order to take into account the other canyon orientations, one should replace w by $w/\sin(\theta)$ in the above expressions, and then multiply the wall fluxes by $\sin(\theta)$. Then let θ_0 be the critical canyon orientation for which the road is no longer in the light, or for which the radiation is minimum when the sun is high enough, i.e.:

$$\theta_0=\arcsin\left(\min\left[\frac{w}{h}\frac{1}{\tan(\lambda)};1\right]\right).$$

Averaging a flux with respect to the canyon orientation is performed with two integrations, one between $\theta=0$ and $\theta=\theta_0$, and the other one between $\theta=\theta_0$ and $\theta=\frac{\pi}{2}$. The direct solar fluxes for walls, roads and roofs then read:

$$S_r^{\Downarrow}=S^{\Downarrow}\left[\frac{2\theta_0}{\pi}-\frac{2}{\pi}\frac{h}{w}\tan(\lambda)(1-\cos(\theta_0))\right], \tag{13}$$

$$S_w^{\Downarrow}=S^{\Downarrow}\left[\frac{w}{h}\left(\frac{1}{2}-\frac{\theta_0}{\pi}\right)+\frac{1}{\pi}\tan(\lambda)(1-\cos(\theta_0))\right], \tag{14}$$

$$S_R^{\Downarrow}=S^{\Downarrow}. \tag{15}$$

Note that from the previous equations, one can deduce the conservation relation $S_r^{\Downarrow}+2\frac{h}{w}S_w^{\Downarrow}=S^{\Downarrow}$.

2.7.2. *Solar Radiation Reflections*

The scattered solar radiation received by the surfaces ($S_\star^{\downarrow}$) is directly deduced from the sky-view factors. Because of the canyon shape and the possible high albedo of the surfaces (white paint, snow), the shortwave radiative budget is computed by resolving a geometric system for an infinite number of reflections. The reflections are assumed to be isotropic: there is no specular reflection in this model. Details of the following calculations are given in Appendix A.

One defines $M_\star$ as the sum of the reflections against the road and wall:

$$M_r=\frac{R_r(0)+(1-\Psi_r)\overline{\alpha_r}\,(R_w(0)+\Psi_w\alpha_w R_r(0))}{1-(1-2\Psi_w)\alpha_w+(1-\Psi_r)\Psi_w\overline{\alpha_r}\alpha_w}, \tag{16}$$

$$M_w=\frac{R_w(0)+\Psi_w\alpha_w R_r(0)}{1-(1-2\Psi_w)\alpha_w+(1-\Psi_r)\Psi_w\overline{\alpha_r}\alpha_w}, \tag{17}$$

with

$$R_r(0)=\overline{\alpha_r}S_r^{\Downarrow}+\overline{\alpha_r}S_r^{\downarrow},$$

$$R_w(0) = \alpha_w S_w^{\Downarrow} + \alpha_w S_w^{\downarrow},$$

$$\overline{\alpha_r} = (1 - \delta_{\text{snow}_r})\alpha_r + \delta_{\text{snow}_r}\alpha_{r_{\text{snow}}}.$$

The total solar radiation absorbed by each of the surface types is:

$$S_r^* = (1 - \alpha_r)S_r^{\Downarrow} + (1 - \alpha_r)S_r^{\downarrow} + (1 - \alpha_r)(1 - \Psi_r)M_w, \tag{18}$$

$$S_w^* = (1 - \alpha_w)S_w^{\Downarrow} + (1 - \alpha_w)S_w^{\downarrow} + (1 - \alpha_w)(1 - 2\Psi_w)M_w + (1 - \alpha_w)\Psi_w M_r, \tag{19}$$

$$S_R^* = (1 - \alpha_R)S_R^{\Downarrow} + (1 - \alpha_R)S_R^{\downarrow}. \tag{20}$$

Note that in these equations, a specific albedo of the surfaces (glass, wet surface) for the direct solar radiation would change only the $\alpha_\star S_\star^{\Downarrow}$ terms.

2.8. ANTHROPOGENIC FLUXES

Due to human activity, heat and moisture are released towards the atmosphere. The two main sources arise from domestic heating and from combustion. Domestic heating is explicitly resolved by supposing a constant internal temperature, whatever the external temperature. The default value is 290.15 K (17 °C). The heat is then released towards the wall/roof surfaces and then towards the atmosphere through the conduction flux formulation.

The combustion source is split into two contributions in the TEB model: traffic and industry. For each, the heat and moisture fluxes, averaged on the town surface (H_{traffic} and LE_{traffic}, H_{industry} and LE_{industry}) are specified by the user (from available information on the town activity).

However, these fluxes do **not** directly modify the surface energy budgets since they are released into the air. The traffic related fluxes will modify the canyon air budget (they are incorporated in Equation (24), see next section). The industry fluxes are assumed to influence the atmosphere directly.

2.9. TURBULENT FLUXES

2.9.1. *Treatment of the Urban Roughness Sublayer, Momentum Fluxes*

In this section, the method to compute the turbulent fluxes between the surfaces and the atmospheric model will be presented. The resolution of the atmospheric model is far too low to be able to represent the urban roughness sublayer motions. The atmospheric models do not usually parameterize the exchange processes in this layer; this is done by using the surface scheme. If the first atmospheric level is outside the roughness sublayer, the traditional surface-layer formulations can be used to compute the turbulent fluxes. The problem is that the roughness sublayer

can have a substantial extension over an urban surface (several tens of metres), and the first level of the atmospheric model (often a couple of tens of metres) is often within it.

It is therefore necessary to take a closer look at the parameterization of the fluxes. Feigenwinter (1999) conducted measurements on a 50-m high mast in the city of Basel (Switzerland), and found that the mechanical properties in the roughness sublayer (such as profiles of velocity variances, non-dimensionalized velocity variances and spectra of wind components) behave similarly to rural surface layers. Furthermore, they concluded that these quantities are quite well-parameterized within the Monin–Obukhov similarity theory, if the local Obukhov length is applied.

Following their results, the TEB scheme computes the *momentum fluxes for the entire urban (or suburban) cover*, with a roughness length formulation and the stability coefficients of Mascart et al. (1995), whatever the relative positions of the atmospheric level and the roughness sublayer depth.

In contrast, Feigenwinter et al. (1999) found that the temperature characteristics, and in particular the turbulent heat flux, cannot be satisfactorily reproduced by the Monin–Obukhov similitude framework. They attribute this discrepancy to 'thermal inhomogeneity and/or different source areas'. The use of one unique surface exchanging heat with the atmosphere (the classical surface-layer approach) becomes debatable.

The approach of the TEB scheme is to suppose that there are *two* major sources of heat from the artificial cover towards the atmosphere, leading to *two* turbulent heat fluxes. These two different surfaces are the *roofs* on the one hand, and the *canyon systems* on the other (see Figure 3). The two flux contributions are averaged relative to their horizontal areas; this is a means of representing the mixing in the urban roughness sublayer.

In suburban environments, the averaging of the sensible and latent heat fluxes from the greenspace artificial parts is similarly supposed to parameterize the roughness sublayer effects.

2.9.2. *Considerations on the Turbulent Transfer of Moisture*

Both for roof and roads, we explicitly assume that the transfer coefficients for turbulent heat and moisture fluxes are identical, but different from that for momentum. Very few direct measurements of turbulent moisture fluxes exist in the literature to check this hypothesis.

Roth and Oke (1993) and Roth (1993) computed statistics from data (including moisture measurements) gathered during 10 days in summer in a suburb of Vancouver. The suburb was composed of 36% artificial cover, and of 64% greenspace. They showed poor correlation between temperature and moisture characteristics, and suggested this was due to spatial inhomogeneity. They concluded that, in their case, the mixing for moisture was less efficient than for heat. However, in the absence of rain during this period, the evaporation arose from the greenspace.

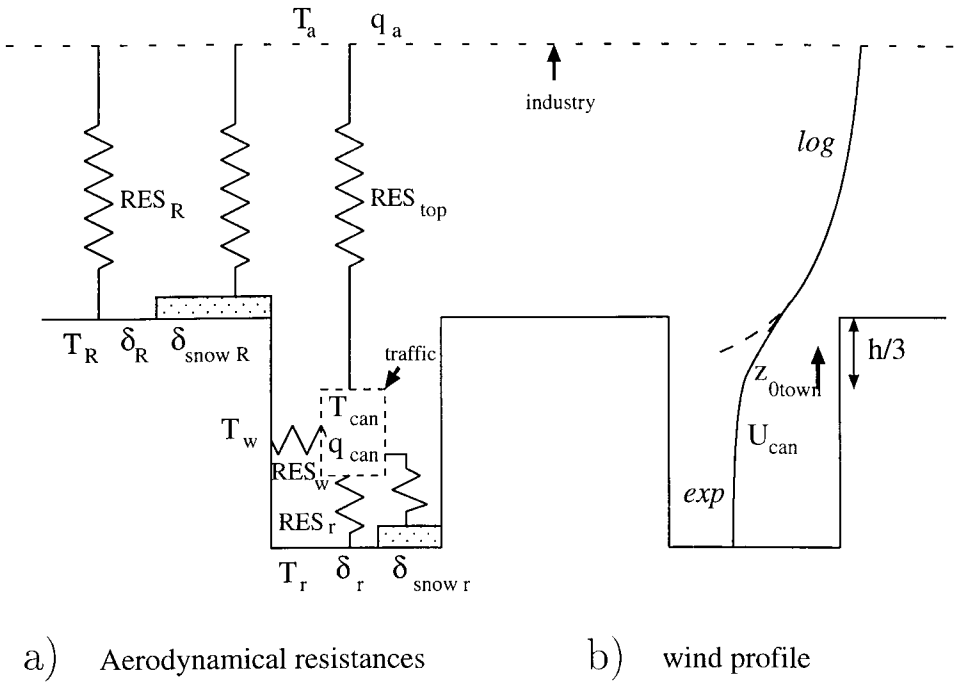

Figure 3. Scheme options for: (a) aerodynamic resistances; (b) wind profile within and above the canyon.

Therefore, it is not possible to draw conclusions about any specific formulation for the moisture flux in the TEB model.

Other latent heat flux data exist, but again during dry periods. Grimmond and Oke (1999a) gathered data from seven North American cities, but five of them are for suburban regions. The two most purely urban cases, central Mexico city, presented in detail in Oke et al. (1999), and an industrial site in Vancouver, show a very small evaporative flux, equal to 4% and 10% of the net radiation (during the day) for the two sites, respectively.

2.9.3. *Roughness Length for Momentum Fluxes*

The momentum fluxes are computed for the entire urban surface. However, one difficulty lies in the determination of the roughness length to use in urban areas. Wieringa (1993) reviewed some experimental roughness length estimations for rather homogeneously built-up areas. Dense low building roughness lengths were found to lie between 0.4 and 0.7 m, and those for regularly-built towns ranged from 0.7 to 1.5 m. In these experiments, they are approximately equal to 1/10 of the house or building heights. Bottema (1997) presents a model computing roughness lengths from building shapes and relative positions (normal or staggered). He found the modeled $z_{0_{\text{town}}}$ to be in agreement with the available measurements. Sensitivity experiments with his model show that the ratio $z_{0_{\text{town}}}/h$ ranges from 0.05 to 0.1,

except for very sparsely built areas. Therefore, as a first approximation, the roughness length in the TEB model is set equal to $z_{0_{\text{town}}} = h/10$, (with an arbitrary limit of 5 m), but it can be specified independently, either from in-situ measurements or from more complex formulations (see, for example, the recent review of Grimmond and Oke, 1999b).

2.9.4. *Heat Fluxes between Roofs and Atmosphere*

The turbulent heat fluxes to/from the roofs are also recovered from classical boundary-layer laws, because the roof heights are supposed uniform, using a roughness length of 0.15 m (as observed by Sturrock and Cole, 1977). Again the stability coefficients of Mascart et al. (1995) are used to compute the aerodynamic resistance RES_R. The effect on temperature and specific humidity of the difference in height between the atmospheric level and the roof level is corrected using the Exner function $\Pi = (p/p_0)^{R_d/C_{pd}}$, where p is the pressure (p_s and p_a are the surface pressure and the first level pressure in the atmospheric model respectively), p_0 is a reference pressure (equal to 1000 hPa), and R_d the gas constant for dry air. We define

$$\hat{T}_a = T_a \Pi_s / \Pi_a,$$

$$\hat{q_a} = q_a q_{\text{sat}}(\hat{T}_a, p_s)/q_{\text{sat}}(T_a, p_a).$$

The heat and moisture turbulent fluxes between roof and atmosphere read:

$$H_R = C_{p_d} \rho_a (\hat{T}_a - T_{\text{can}})/\text{RES}_R,$$

$$LE_R = L_v \rho_a (\hat{q}_a - q_{\text{can}})/\text{RES}_R,$$

where ρ_a is the air density at first atmospheric level, and C_{p_d} the heat capacity of dry air.

2.9.5. *Wind Inside the Canyon*

The computation of the wind inside the canyon is necessary to estimate the heat fluxes between the surfaces and the canyon. The vertical wind speed along the walls, W_{can}, as well as the horizontal wind speed in the canyon, U_{can}, must be defined. Rotach (1995) presents turbulence measurements in and above a road in the center of Zurich (Switzerland), for which the canyon aspect ratio is $h/w \approx 1$. Rotach (1995) observed that the standard deviation of the vertical wind speed, σ_w, in the upper part of the canyon, is almost equal to the friction velocity u_*, whatever the stability or wind direction above. Feigenwinter et al. (1999) finds that σ_w/u_* is, on the contrary, increasing with height for unstable conditions. However, their value of σ_w/u_* near the roof level (extrapolated using a Monin–Obukhov function) was approximately 1.15, which is of the same order of magnitude as the Rotach (1995) results. They also found that for stable to weakly unstable conditions, u_*

presents a maximum between the roughness sublayer and the inertial sublayer above. However, u_* does not depart by more than 10% from its value in the inertial sublayer, and is assumed constant with height in the scheme.

Then, assuming that all this holds true for other canyon aspect ratios, the vertical wind speed along the walls reads:

$$W_{\text{can}} = u_* = \sqrt{C_d}|\mathbf{U}_a|, \tag{21}$$

where $\mathbf{U}_a$ is the wind velocity at the first atmospheric model level. The drag coefficient, C_d, is computed from the temperatures and humidities in and above the canyon, and from the roughness length, $z_{0_{\text{town}}}$, taking into account the stability effects according to Mascart et al. (1995).

The horizontal wind speed, U_{can}, is estimated at half the height of the canyon. First, the horizontal wind speed at the top of the canyon is deduced from the logarithmic law above it (Figure 3, right side), and the displacement height is equal to two thirds of the building height from the road surface (i.e., at $h/3$ under the roof level, which is the zero height of the atmospheric model, a classical assumption for plant canopies). Furthermore, in order to consider all canyon orientations, and since only the along canyon wind is considered, an integration over 360° is performed. At canyon top, this gives:

$$U_{\text{top}} = \frac{2}{\pi} \frac{\ln\left(\frac{h/3}{z_{0_{\text{town}}}}\right)}{\ln\left(\frac{\Delta z + h/3}{z_{0_{\text{town}}}}\right)} |\mathbf{U}_a|,$$

where Δz is the height of the first atmospheric model level above the roofs.

To calculate U_{can}, a vertical profile of the wind inside the canyon, is assumed. An exponential form is chosen, as is done in vegetation canopies, e.g., Arya (1988). Such a profile applied at half-height gives:

$$U_{\text{can}} = U_{\text{top}} \exp(-N/2),$$

where N must be determined. Rotach (1995) finds from his case study ($h/w = 1$), that $U_{\text{can}} \approx 0.75 U_{\text{top}}$. Studies in corn fields ($h/w \sim 4$), which could be assimilated to narrow streets, give $U_{\text{can}} \approx 0.4 U_{\text{top}}$ (Arya, 1988). Therefore, the parameter $N = 0.5 h/w$ should be appropriate. Then

$$U_{\text{can}} = \frac{2}{\pi} \exp\left(-\frac{1}{4}\frac{h}{w}\right) \frac{\ln\left(\frac{h/3}{z_{0_{\text{town}}}}\right)}{\ln\left(\frac{\Delta z + h/3}{z_{0_{\text{town}}}}\right)} |\mathbf{U}_a|. \tag{22}$$

2.9.6. *Sensible and Latent Heat Fluxes in the Canyon*

The turbulent heat fluxes between the canyon air and the atmosphere are computed from the temperature and humidity inside the canyon. The fluxes between surfaces

and canyon air follow an empirical formulation. The air characteristics inside the canyon are deduced from the continuity between the fluxes arising from the surfaces and the flux with the atmosphere (inspired by the vegetation canopy scheme of Deardorff, 1978).

The heat fluxes are used in the energy budget conservation equations involving the surface temperatures. This is why a precise approach has been chosen, specific to each surface. Figure 3 displays a summary of the TEB options.

Fluxes between canyon air and atmosphere

Above the canyon, the fluxes are estimated from classical surface boundary-layer laws. However, in these formulae, the air characteristics in the canyon (T_{can} and q_{can}) are used instead of the surface characteristics. The aerodynamic resistance above the canyon, called RES_{top}, is calculated with $z_{0_{\text{town}}}$ using the stability coefficients of Mascart et al. (1995) (this formulation leads to different drag coefficients for momentum fluxes and for heat or moisture fluxes).

The heat and moisture turbulent fluxes between canyon and atmosphere then read:

$$H_{\text{top}} = C_{p_d}\rho_a(\hat{T}_a - T_{\text{can}})/\text{RES}_{\text{top}},$$

$$LE_{\text{top}} = L_v\rho_a(\hat{q}_a - q_{\text{can}})/\text{RES}_{\text{top}}.$$

Fluxes between walls, roads and canyon air

Between the canyon surfaces (road and walls) and the canyon air, the Rowley et al. (1930) and Rowley and Eckley (1932) aerodynamic formulations are used. They were obtained from in-situ measurements; these formulae are also used in the canyon circulation model of Mills (1993). Other formulations of similar form exist in the literature (see e.g., Sturrock and Cole, 1977, either from wind-tunnel or in-situ measurements).

For simplicity, the same value is chosen for both road and walls. The resistance is independent of the stability inside or above the canyon. It reads:

$$\text{RES}_r = \text{RES}_w = \left(11.8 + 4.2\sqrt{U_{\text{can}}^2 + W_{\text{can}}^2}\right)^{-1}. \tag{23}$$

Finally, the heat fluxes between the canyon surfaces and the canyon air read:

$$H_r = C_{p_d}\rho_a(T_r - T_{\text{can}})/\text{RES}_r,$$

$$H_w = C_{p_d}\rho_a(T_w - T_{\text{can}})/\text{RES}_w,$$

$$LE_r = L_v\rho_a\delta_r(q_{\text{sat}}(T_r, p_s) - q_{\text{can}})/\text{RES}_r,$$

$$LE_w = 0.$$

Notice the form of the latent heat flux, where the fraction of wet road, δ_r, is applied outside of the parentheses. Therefore, the evaporation from the surface occurs when $q_{\rm sat}(T_r) > q_a$, even if very little water remains. The same humidity treatment is performed for roofs.

2.9.7. *Canyon Temperature and Humidity*

These quantities can be considered as output of a meteorological forecast. They are computed diagnostically: the equilibrium between thermodynamic fluxes for the canyon air is assumed to be valid at each time step. *The anthropogenic flux due to traffic is also taken into account*. Note that in this formula, $H_{\rm traffic}$, representative of the whole urban surface, has been scaled to the road surface.

$$H_{\rm top} = (1 - \delta_{{\rm snow}_r}) H_r + \frac{2h}{w} H_w + H_{\rm traffic} \frac{1}{1 - a_{\rm bld}} + \delta_{{\rm snow}_r} H_{{\rm snow}_r}, \tag{24}$$

$$LE_{\rm top} = (1 - \delta_{{\rm snow}_r}) LE_r + LE_{\rm traffic} \frac{1}{1 - a_{\rm bld}} + \delta_{{\rm snow}_r} LE_{{\rm snow}_r}. \tag{25}$$

Then

$$T_{\rm can} = \frac{(1 - \delta_{{\rm snow}_r}) \frac{T_r}{{\rm RES}_r} + \frac{2h}{w} \frac{T_w}{{\rm RES}_w} + \frac{\hat{T}_a}{{\rm RES}_{\rm top}} + \frac{H_{\rm traffic}}{C_{p_d} \rho_a (1 - a_{\rm bld})} + \delta_{{\rm snow}_r} \frac{H_{{\rm snow}_r}}{C_{p_d} \rho_a}}{(1 - \delta_{{\rm snow}_r}) \frac{1}{{\rm RES}_r} + \frac{2h}{w} \frac{1}{{\rm RES}_w} + \frac{1}{{\rm RES}_{\rm top}}}, \tag{26}$$

and,

$$q_{\rm can} = \frac{(1 - \delta_{{\rm snow}_r}) \frac{\delta_r q_{\rm sat}(T_r, p_s)}{{\rm RES}_r} + \frac{\hat{q}_a}{{\rm RES}_{\rm top}} + \frac{LE_{\rm traffic}}{L_v \rho_a (1 - a_{\rm bld})} + \delta_{{\rm snow}_r} \frac{LE_{{\rm snow}_r}}{L_v \rho_a}}{(1 - \delta_{{\rm snow}_r}) \frac{\delta_r}{{\rm RES}_r} + \frac{1}{{\rm RES}_{\rm top}}}. \tag{27}$$

2.9.8. *Averaged Fluxes at Town Scale*

As mentioned above, the averaging operation performed to obtain the turbulent fluxes at town scale is in itself a way to solve the problem of the roughness sublayer: It mimics the mixing of the different sources of turbulent heat fluxes, and then produces *fluxes that are representative of the upper part of the surface layer*, above the roughness sublayer. The energy fluxes released by the industrial activities are also added at this stage.

The total heat fluxes from the artificial material areas towards the atmosphere are then:

$$H_{\rm town} = a_{\rm bld} H_R + (1 - a_{\rm bld}) H_{\rm top} + H_{\rm industry}, \tag{28}$$

$$LE_{\text{town}} = a_{\text{bld}} LE_R + (1 - a_{\text{bld}}) LE_{\text{top}} + LE_{\text{industry}}. \quad (29)$$

In order to have the total turbulent fluxes H, LE from the surface towards the atmospheric model, these fluxes should be averaged with those computed by the vegetation scheme for the other land surfaces (city parks, gardens, fields, forest, bare soil) and those from water covered surfaces (rivers, lakes, sea).

3. Validation of the Radiative Aspects

3.1. HEAT ISLAND AT NIGHT

The results of the TEB model are now compared to the heat island episode in the Grand-view district of Vancouver (Nunez and Oke, 1976, 1977; simulated in Johnson et al., 1991). This is a calm clear-sky night. This case allows the validation of the longwave budget and wall and road surface temperature evolutions (then the conduction fluxes), both for the road and walls. The temperature profile is assumed to be neutral (no thermal turbulent fluxes between the canyon and the atmosphere). However, turbulent exchanges exist between walls and roads through the canyon air. This is the main difference with respect to the SHIM model of Johnson et al. (1991). Another important difference is the explicit conduction flux treatment in the TEB model, instead of the force-restore method in their model.

The urban characteristics are adapted from Johnson et al. (1991). The road sky-view factor is still 0.51, but the wall sky-view factors must be changed in the TEB model, since they are identical for both walls, and are averaged. The same initial temperatures are chosen. The thermal conductivities and heat capacities⋆ are estimated in order to keep the same thermal admittance ($\mu = (\lambda C)^{\frac{1}{2}}$) as in Johnson et al. (1991). The wall depth fits the diurnal penetration depth used in the force-restore method: $D = (\frac{\lambda \tau_{\text{day}}}{C\pi})^{\frac{1}{2}}$. The downward radiative fluxes are proportional to the air temperature at the fourth power, starting from 339 W m^{-2}.

Figure 4 shows the results of the TEB model, for road surface temperature and longwave fluxes, compared with those of Johnson et al. (1991). The comparison is performed for the road surface temperature and longwave budget, and for the wall surface temperatures and longwave budgets.

The two models give very similar results, even with the slightly simpler TEB geometry. The net radiation fluxes are correctly reproduced (differences less than 10 W m^{-2}), and surface temperatures depart by less than 1 K from the observed near-surface air temperatures. Note also that the net radiation budget for a horizontal surface exposed to the sky starts at -64 W m^{-2} and ends at -45 W m^{-2}, and surface temperature ends 3 K lower than the canyon case (not shown). The exchange of sensible heat flux between the walls and road is on the order of 7 W m^{-2}

⋆ $C_w = 10^6$ J m^{-3} K^{-1}; $\lambda_w = 0.81$ W m^{-1} K^{-1}; $C_r = 1.94 \times 10^6$ J m^{-3} K^{-1}; $\lambda_r = 1.0103$ W m^{-1} K^{-1}).

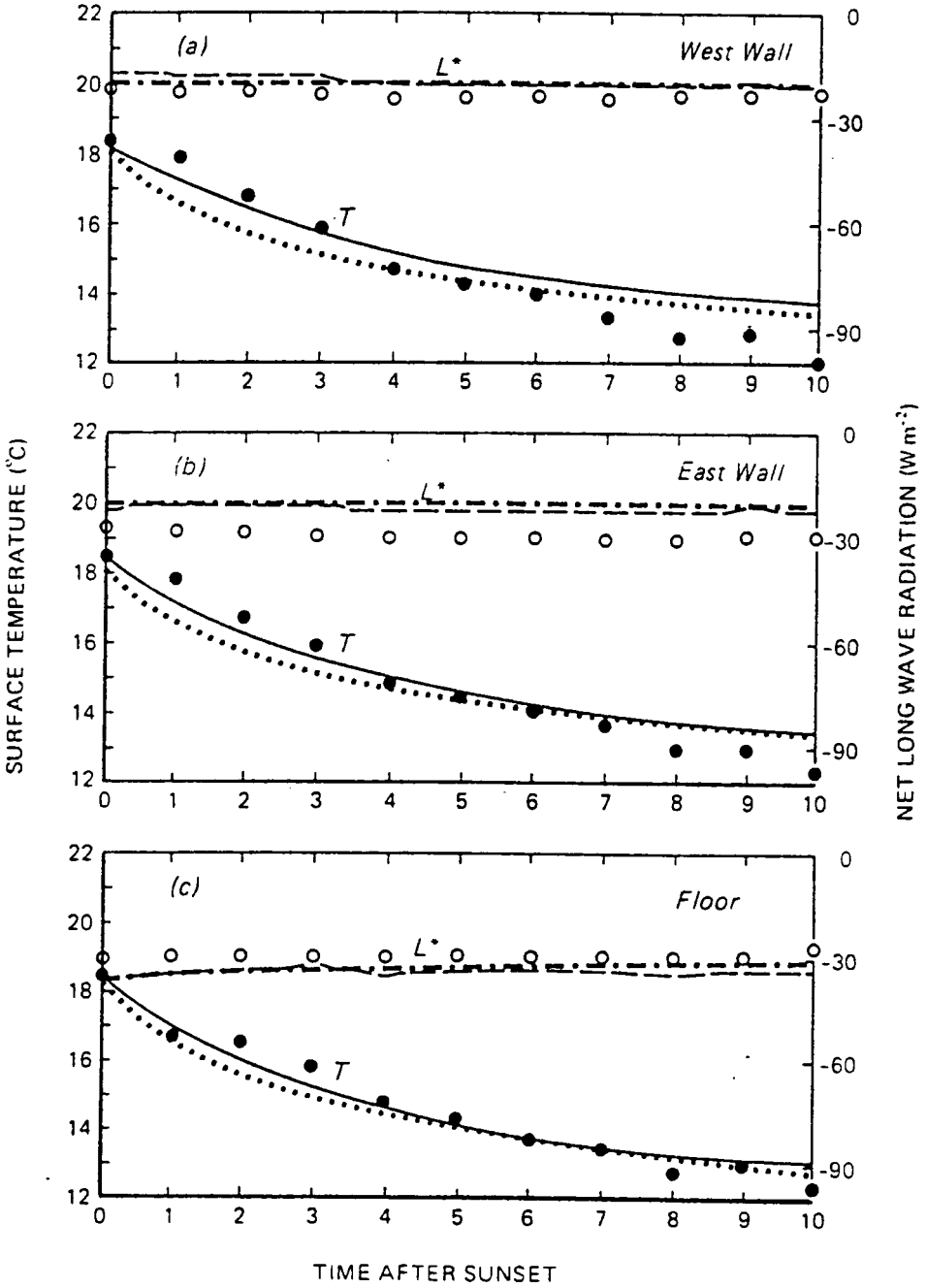

Figure 4. Comparison between modelled surface temperature (full line: SHIM; dotted line: TEB) and net longwave radiation (dashed line: SHIM; dashed-dotted line: TEB) and measurements (dots): (a) west wall, (b) east wall, (c) floor. The TEB model results are identical for both walls. Night time situation of September 9/10 1973 (figure from Johnson et al., 1991; figure 5).

(from the wall towards the road). This small value explains the similarities between SHIM and TEB for such ideal conditions.

3.2. SHORTWAVE BUDGET

The relations (18)–(20) parameterize the shortwave trapping by the city geometry. Experimental data exist to validate this representation – Aida (1982) built four models of urban structure with cubic concrete blocks of 15-cm width, and measured the solar radiation reflected by this surface. Model 0 is the flat reference surface; models 1 and 2 consist, respectively, of canyons oriented north-south and east-west; finally, model 3 contains north-south and east-west crossing canyons. The canyons and block aspect ratios are equal to unity. These geometries fortunately are close to the one chosen for the TEB model. Models 1 and 2 should be together represented in TEB by 50% roof and 50% road; model 3 contains only 25% roofs.

Figure 5 (from Aida, 1982) shows the measurements of surface albedo, as dots, compared with the total, effective albedo (at the first model level) obtained from the direct shortwave TEB computation results. The roof albedo is adjusted using Aida model 0 summer observations. It varies between 0.36 and more than 0.50, depending on solar zenith angle. The albedo for road and wall surfaces is taken as a constant, equal to 0.40, because all reflections are supposed isotropic for these surfaces.

The observed albedo for parallel canyons does not depend on direction; they show an important albedo decrease, compared to the flat reference surface (model 0). The results of the TEB model nearly coincide with them. This validates both the orientation-averaged calculations for shortwave radiation, at least at urban-scale, and the multiple reflection computations. The TEB model slightly overestimates the increase of radiative trapping when crossing roads are considered (Aida model 3). This probably arises from the hypothesis that roads are far longer than wide, while it is clearly not the case in the Aida model. However, the difference is limited to a few percent on the town albedo, five times less than the trapping effect for the Aida study.

The effect of canyon shape on the effective canyon albedo computed in TEB (i.e., the ratio of reflected solar energy from the canyon over the downward solar energy) is now investigated. Figure 6 displays the effective albedo as a function of canyon shape and zenith angle, for surfaces with albedos of 40%, as above. For a flat surface, the albedo is then 40%, but decreases rapidly as the canyon shape h/w increases: for $h/w = 1$, the albedo is as low as 18%, and between 10 and 2% for $h/w = 3$. The elevation of the sun above the horizon has no effect for $h/w = 1$ (Aida case); the dependence upon zenith angle found above is explained by the flat surface albedo only. Tall buildings further increase the trapping effect, with greater efficiency for high sun. The effective albedo always behaves as in Figure 6

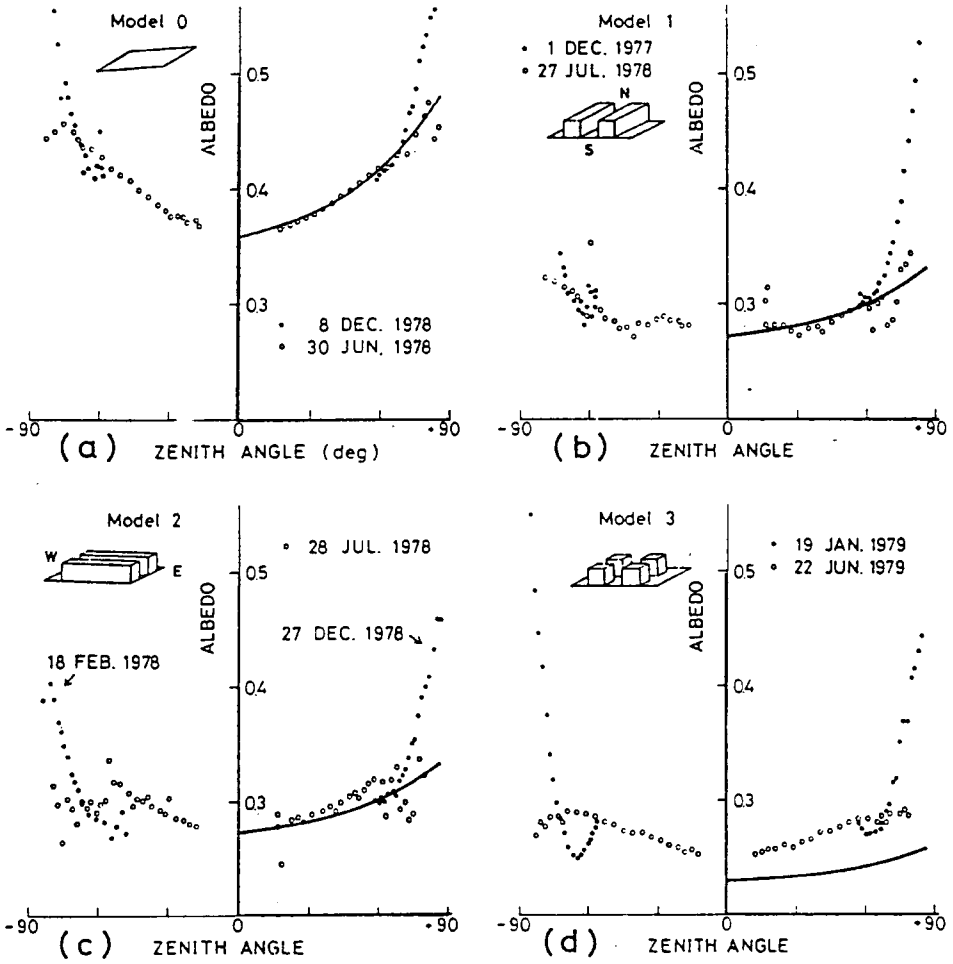

Figure 5. Urban albedo as measured by Aida (dots) for various models (see inset) and parameterized by the TEB model (superimposed lines): (a) roof albedo fitted on Aida observations for a flat concrete surface; (b) and (c) albedo parameterized for uni-directional Aida models 1 and 2; (d) albedo parameterized for crossing-roads Aida model 3; h/w = 1. Road and wall albedos are equal to 0.40 in TEB computations. Road fraction is equal to 50% in models 1 and 2, and 75% in model 3. (figure from Aida, 1982; figure 5).

for identical wall and road albedos (not shown), even if the singular point with no effect of zenith angle is not found for the same canyon aspect ratio.

The albedo behaviour is different for more realistic albedo values, in the presence of bright walls and dark roads (for example, with albedos of 25% and 8% respectively, Figure 7). For the sun at the zenith, the albedo decrease is similar as above, but when the sun directly illuminates the walls, the albedo decreases slower with respect to canyon shape, and can even increase if the sun is low enough. When $h/w = 1$, the effective albedo is as high as the flat road albedo for the sun

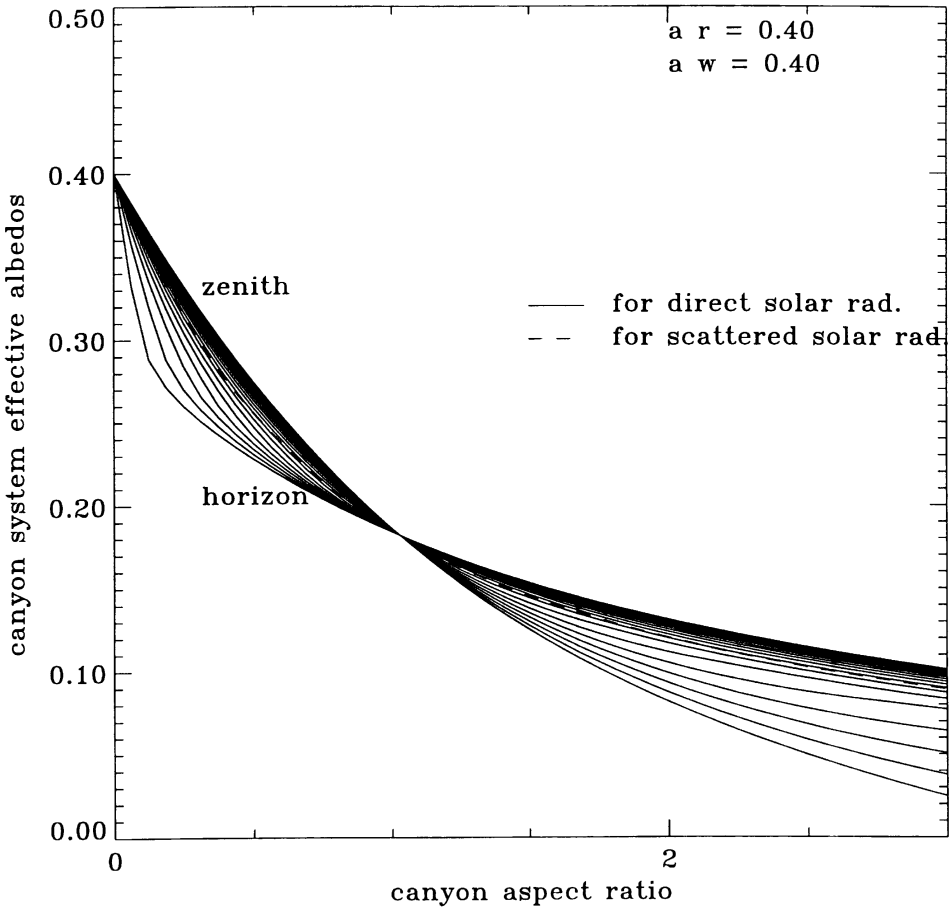

Figure 6. Canyon effective albedo as a function of canyon shape and solar zenith angle (from zenith to 5° above horizon every 5°). Effective albedo for scattered shortwave flux is displayed using a dashed line. Road and wall surface albedos are both equal to 40%. Note that the part of the albedo due to the roofs is not present in this figure.

just above the horizon. Note that the effective albedo with the sun at the zenith is always much smaller than when the sun is low. Therefore, trapping effects will be important in summer, because the sun is high at noon, but the weaker solar energy will not be captured as efficiently in winter.

At this stage, some of the TEB model basics – geometry, radiative (both infrared and solar) scheme and conduction formulation – have been validated against observations. The two main uncertainties remaining are the turbulent flux formulation, and the hydrological aspects. These will be addressed in the following section through sensitivity experiments.

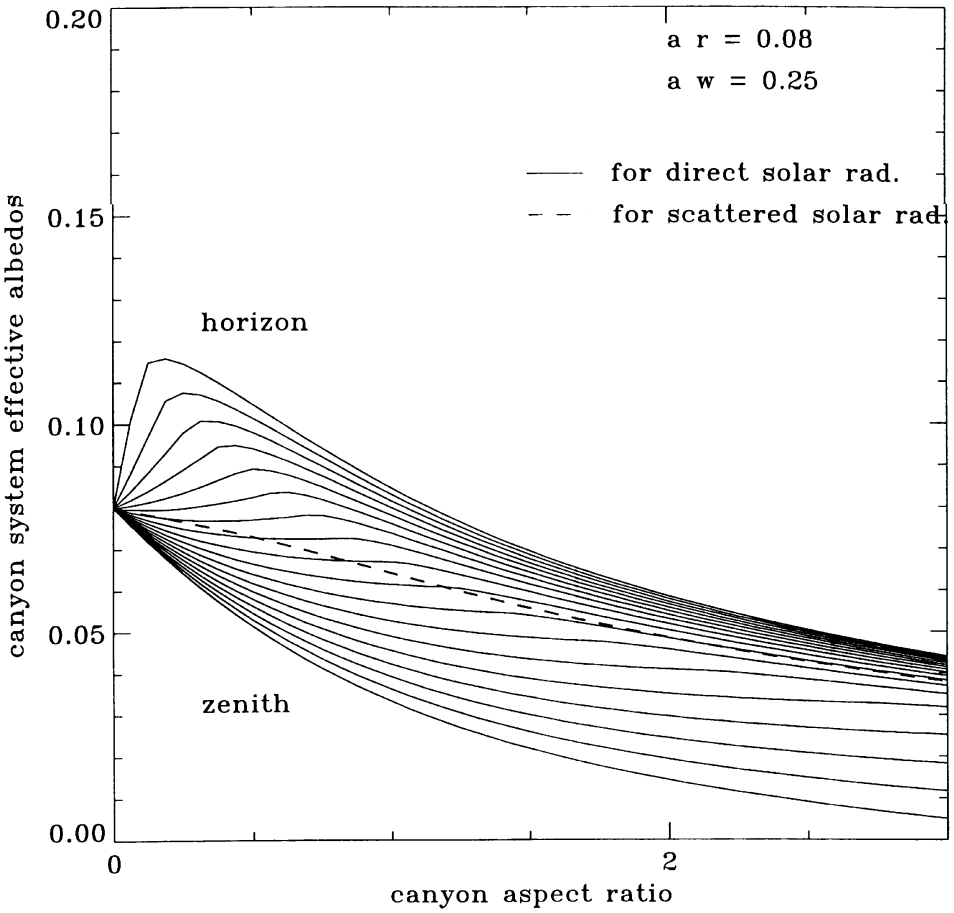

Figure 7. As in Figure 6, except that walls are bright (albedo is 25%) and roads are dark (albedo is 8%).

4. Sensitivity Experiments

In this section, the TEB model is run using several long meteorological forcing time series in order to investigate its ability to represent the energetics of the urban atmosphere. This allows the study of the scheme response to a large variety of weather conditions encountered in the real atmosphere. Unfortunately, such data (with forcing, observed surface temperatures and area-averaged energy fluxes) are not available for densely urbanized areas. Therefore, the measurements of two field experiments dedicated to vegetation surface scheme studies are used as replacements. The first one is the Hapex Mobilhy case (André et al., 1988), which took place in southern France in 1986. It is representative of a mid-latitude oceanic climate region. The second one is the first year of the 18 year-long Valdai experiment (Russia, near Moscow, see Schlosser et al., 1997), representing a continental

TABLE III

Urban characteristics for the sensitivity experiments. Only the parameters different from the reference experiment are shown. Composition of the layers is displayed with the corresponding layer thickness.

Experiment name → parameter ↓	Reference	Buildings	Suburban	Insulated	Insulated, Ti
a_{town}	100%		70%		
a_{bld}	50%				
h/w	1	3	0.5		
$z_{0_{\text{town}}}$ (m)	5		1		
$T_{i_{\text{bld}}}$ (K)	290.15				Variable
d_{R_1} (dense concrete) (cm)	5				
d_{R_2} (aerated concrete) (cm)	40				
d_{R_3} (insulation layer) (cm)	5			20	20
d_{w_1} (dense concrete) (cm)	2				
d_{w_2} (aerated concrete) (cm)	12.5				
d_{w_3} (insulation layer) (cm)	2			8	8
d_{r_1} (asphalt) (cm)	5				
d_{r_2} (dry soil) (cm)	10				
d_{r_3} (dry soil) (cm)	100				
α_R	15%				
α_w	25%				
α_r	8%				
ϵ_R	90%				
ϵ_w	85%				
ϵ_r	94%				

climate. Two comments are necessary: first, this is not a validation of the scheme because no urban flux outputs or surface temperatures are available for these data sets. Second, the temperature and downward radiative fluxes can be questionable during heat island episodes. In anticyclonic periods, the countryside forcing temperature data are probably lower than what would be the case in reality over the city centres in these regions, since air is not advected from the countryside but representative of the urban area. Consequently, the sensible heat fluxes will be overestimated during calm cold events. They are probably correct if the wind is large enough. This limitation probably only makes the city representative of areas a little further north of the actual study areas, and does not alter the conclusions drawn from the study.

4.1. OCEANIC CLIMATE: THE HAPEX-MOBILHY CASE

A reference run is performed with the characteristics described in Table III. It represents a medium sized city, with streets as wide as the buildings are high; the roof and road fractions are the same. The walls and roofs are made with concrete, with a tiny insulation layer in the interior. The thermal parameters for wall and roofs are from Oke (1987), those for roads (one asphalt layer and two dry soil layers) are from Mills (1993). Note that road and wall albedos are the same as those used in the Figure 7 discussion (Section 3.2). A small anthropogenic flux is added for both the car traffic and industry (20 W m^{-2} during the day, and 5 W m^{-2} during the night). For the vegetation part of the suburban environment run (Subsection 4.1.3), the ISBA scheme is used (Noilhan and Planton, 1989). The run starts on 1 January 1986 and lasts one year.

4.1.1. *Diurnal Cycles*

The mean diurnal cycles of surface fluxes for March, June, September and December are shown in Figure 8. The diurnal cycles separate into two categories: cold cycle (December) and temperate or warm cycle (others months).

In the warm season, the radiative loss during the night is mainly counterbalanced by the building heat release, with small heat turbulent fluxes. During the morning, the heat storage in roads and buildings is the main budget term. Then the turbulent sensible heat flux becomes dominant, and its maximum is two to three times larger than the ground flux. This hysteresis behaviour is well known in urban climatology (see e.g., Grimmond and Oke, 1995; Grimmond et al., 1991; or Ross and Oke, 1988). The latent heat flux is very small compared to the others. It is maximum in the morning due to the evaporation of rainfall or dew that accumulated during the night, but is very low in the afternoon.

The partition between the turbulent heat flux and ground flux during the day is modified when the building height is larger, as can be seen if the canyon aspect ratio is increased to $h/w = 3$ (Figure 9). The storage efficiency is improved by the increase of wall surface, and the energy amount available for turbulent heat flux is reduced. In our case, the ground fluxes becomes the dominant term of the daytime budget in September. Such an effect of dampening of the turbulent flux has been observed in Mexico, and is documented by Oke et al. (1999). During their observation period (seven days) the daytime G/Q^* is as large as 0.58, while H/Q^* is only 0.38.

During the cold season (Figure 8), this budget cycle is modified by the heat release/storage by the buildings. During the day, the turbulent heat flux is reduced because of the small solar input, but the main difference occurs during the night. The air temperature being much smaller than the building interior, the heat release is more important than the longwave loss, and a turbulent heat flux towards the atmosphere is generated. This phenomenon is greatly enhanced in the continental case (see Section 4.2).

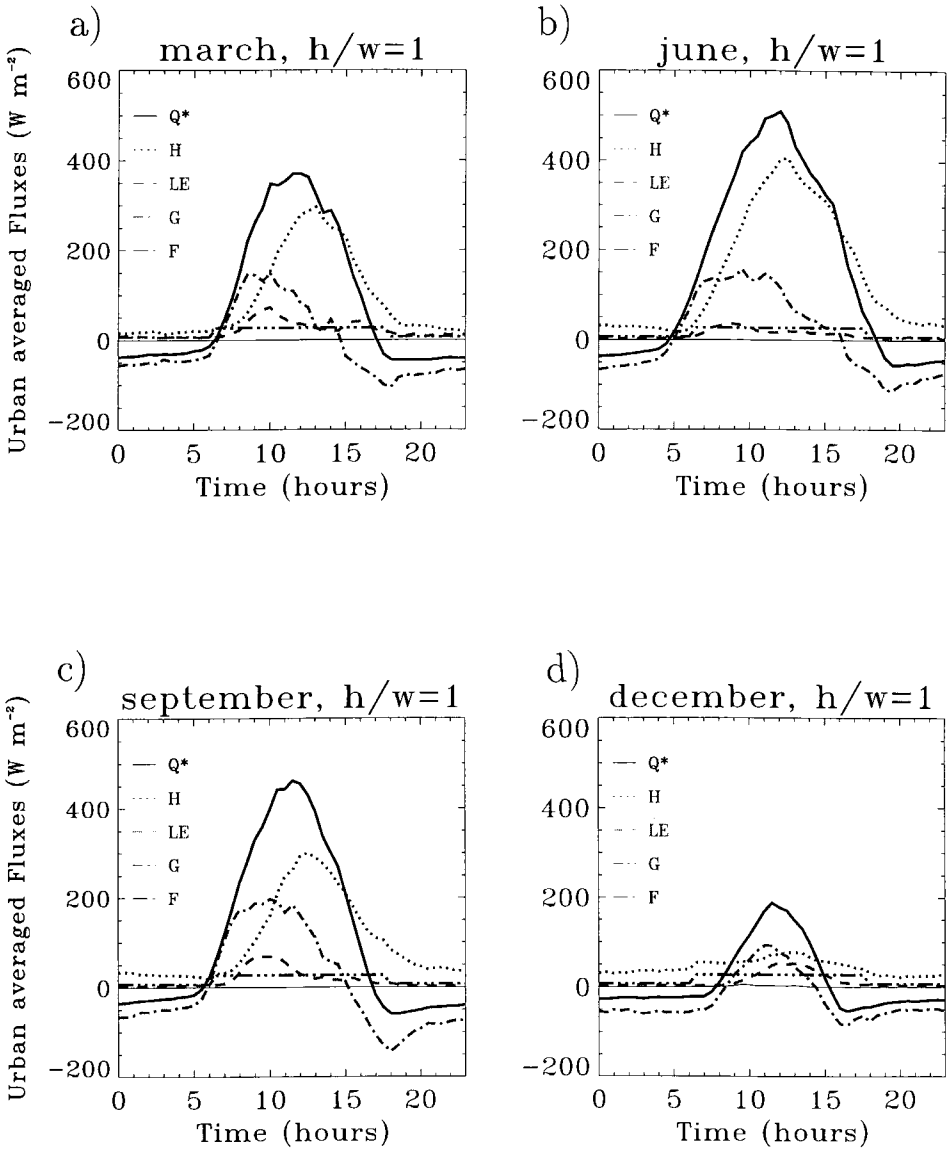

Figure 8. Monthly averaged energy budget diurnal cycles for the reference simulation for the HAPEX-MOBILHY case ((a) March; (b) June; (c) September; (d) December). Sources are: Net radiation (Q^*, full line); Anthropogenic combustion sources (F, dashed-triple dot). Sinks are: Sensible heat flux (H, dotted), latent heat flux (LE, dashed), ground fluxes (G, dashed-dot). Negative ground flux represents heating by the buildings' interior.

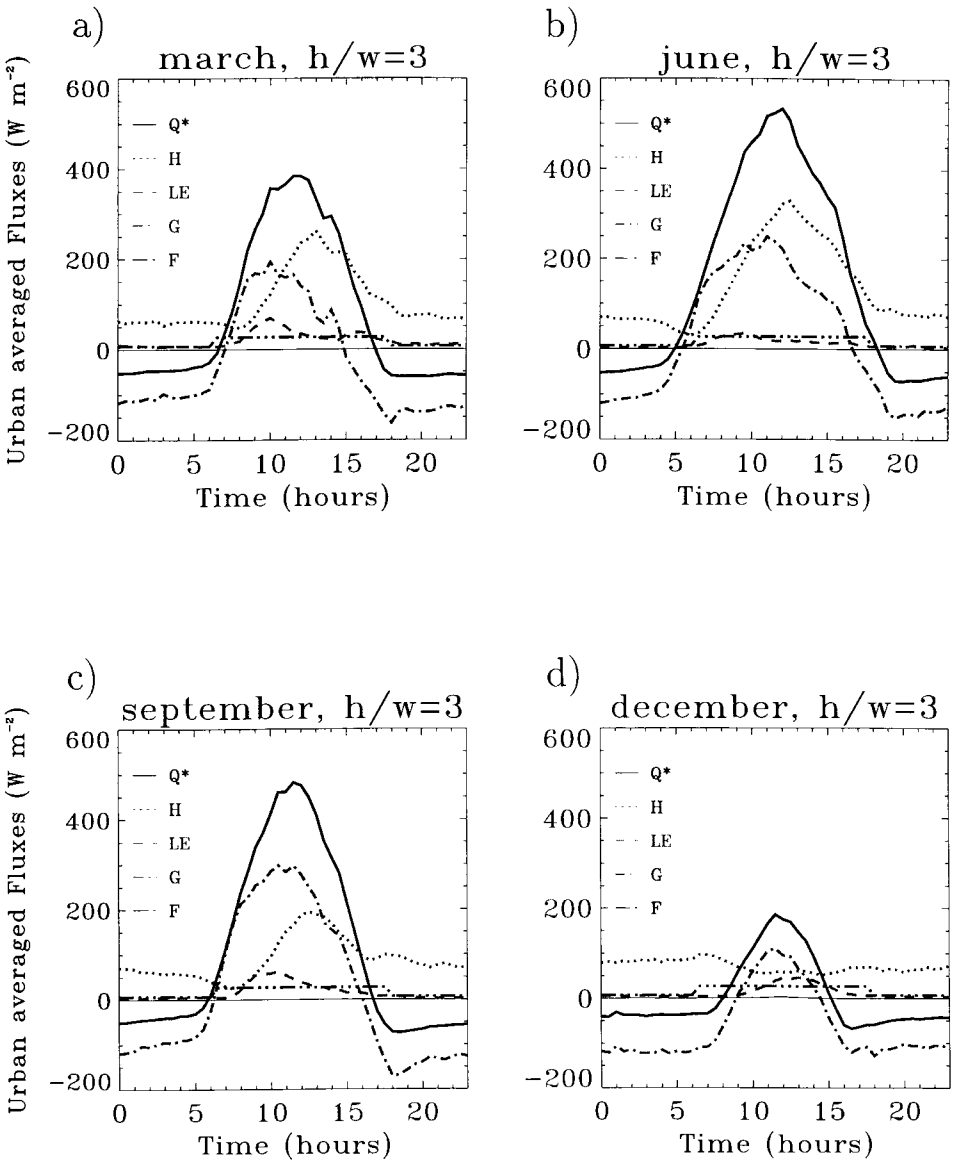

Figure 9. Monthly averaged energy budget diurnal cycles for the high building simulation for the HAPEX-MOBILHY case: (a) March; (b) June; (c) September; (d) December. Same line convention as in Figure 8.

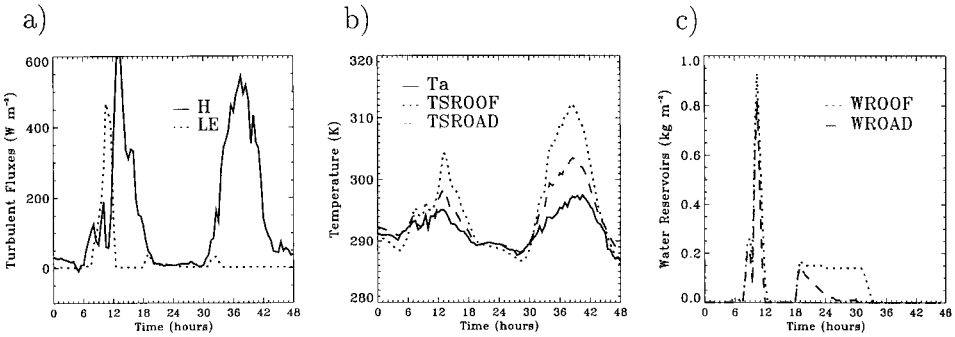

Figure 10. Two consecutive summer days in the reference simulation for the HAPEX-MOBILHY case (from July 6, 0000 UTC to July 8, 0000 UTC). A rain shower occurs in the morning and evening of the first day: (a) sensible heat flux (solid line, W m^{-2}) and latent heat flux (dots, W m^{-2}); (b) air temperature (solid line, K), roof surface temperature (dots, K), road surface temperature (dashed, K); (c) roof surface reservoir (dots, kg m^{-2}), road surface reservoir (dashed, kg m^{-2}).

This sensitivity experiment shows that the TEB model is then able to construct a realistic diurnal cycle, without any ad-hoc assumption about the time hysteresis between ground and turbulent heat fluxes. It is possible to reproduce conditions where the heat storage during the day is sufficient to limit or even overtake the turbulent heat flux. It also suggests that the latent heat flux can be negligible in models dedicated to long term urban energy studies.

4.1.2. *Shower Event*

The fact that the latent heat flux is much lower on average than the other contributions to the energy budget does not mean that it is negligible *when smaller time scales are considered*. For example, two consecutive days in July are presented in Figure 10. A rain shower occurs during the morning of the first day, and a relatively weaker one in the evening of the same day. The downward solar radiation is almost the same during these two days (maxima are 850 W m^{-2} at noon, not shown).

During the first day, the latent heat flux is the main energy sink in the budget, three times larger than the sensible heat flux. One millimetre of water is evaporated in three hours, similarly on roofs and streets, until all the water has been consumed. This has an effect on surface temperatures, which are unable to rise significantly until water is evaporated.

The evaporation of the evening shower during the night is negligible for roofs, but not for roads (20 W m^{-2}), even if much smaller than during the day. This is due to the exchange formulation, which allows mixing between the surface and the canyon air, and then transport towards the atmosphere. This explains the decrease of the water reservoir on the roads during the night, though the difference was not present during the day.

The second day is almost dry, and shows much higher temperatures for a similar input radiation. Differences of 5 K for roads and 10 K for roofs are simulated the

second day. To our knowledge, no direct measurements of latent heat fluxes over towns are available for rainy or wet surface conditions; few such measurements exist, and only for dry conditions. Grimmond and Oke (1999a) presents urban and suburban energy budgets for seven north-American cities, but without rain events. However, a combined measurement of area-averaged sensible heat flux and surface temperatures could probably be used to estimate the instantaneous latent heat flux after shower events. At the very least, the model temperature features could be compared to observations, providing an indirect validation of the simulated fluxes.

4.1.3. *Annual Cycle and Sensitivity Experiment*

Sensitivity experiments on town geometry are performed (buildings, medium town, suburban area). The annual cycles are displayed in Figure 11.

An important feature is the similarity of the net radiative flux for high buildings ($h/w = 3$) or medium sized ones ($h/w = 1$). This suggests that most of the radiative trapping (both for shortwave and longwave) occurs for medium buildings. The similarity in net shortwave radiation trapping for medium or high cities can be explained from Figure 7: for this albedo setting, the canyon shape increase between $h/w = 1$ and $h/w = 3$ is a little more efficient for a low or high sun than for the mid-sky sun encountered in mid-latitude summers.

The building height has a significant impact on the sensible heat flux, courtesy of the larger surface exchange. In winter, early spring and late autumn periods, the sensible heat flux is *larger* than the net radiation. The energy is supplied by the domestic heating (negative G terms on the figures). In our case it reaches 30 W m^{-2} for $h/w = 1$, and 70 W m^{-2} for $h/w = 3$. In summer, the diurnally averaged ground flux is near zero, and almost all the net radiation is transferred as sensible heat flux. Such values of anthropogenic fluxes are compatible with those listed in Oke (1988) for mid-latitude cities (from 20 to 40 W m^{-2} for year averages).

In the suburban environment, due to the fraction of vegetation present, the latent heat flux is increased and the sensible heat flux reduced (up to 40 W m^{-2} loss). One can note that the net radiation is lower (10 W m^{-2}), because radiative trapping is reduced.

Comparison of the annual cycle reproduced for countryside crops or bare soil is shown in Figure 12; the main difference is the much smaller radiative trapping. The contribution due to shortwave radiation trapping is visible in summer (30–40 W m^{-2} less than in the reference experiment). The smaller infrared input is compensated by lower temperatures at night (not shown), comparable to roof temperatures. When vegetation is present, the latent heat flux is the main component of the energy budget, the plant roots extracting water from deep within the soil and evaporating this in warm seasons. The energetic behaviour of a bare soil layer (here 20 cm deep) is much closer to the town surface energy budget, especially the suburban one. This is why the urban canopy is, for the time being, often simulated by bare soil in atmospheric research models. It is shown here that it is a good enough approximation for climatic or large-scale runs, once the radiative properties of the

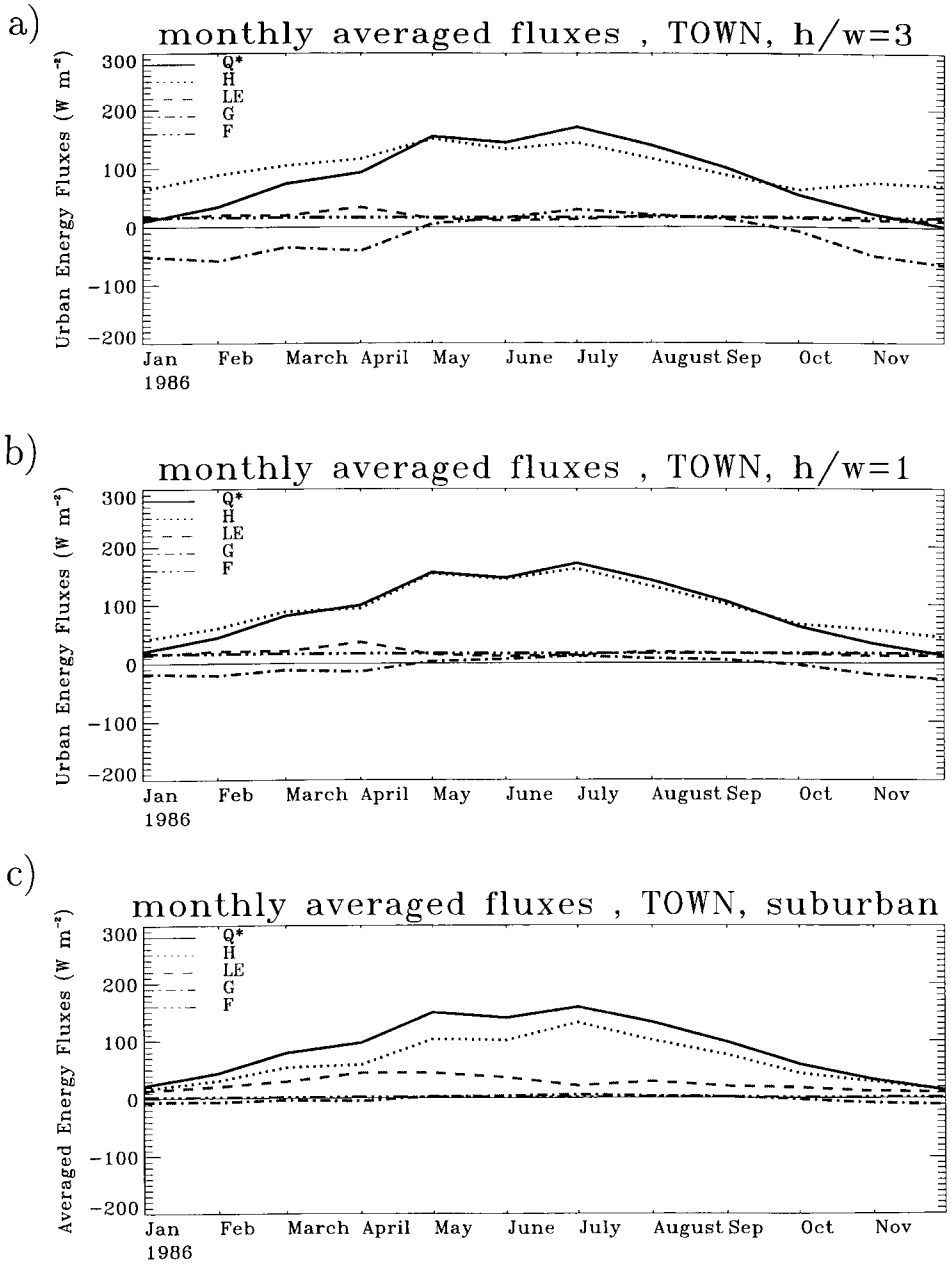

Figure 11. HAPEX-MOBILHY case: monthly averaged energy budget for three city types: (a) high buildings; (b) medium size city (reference simulation); (c) suburban area. Same line convention as in Figure 8.

soil are tuned to reproduce the trapping. An estimation of the anthropogenic flux by domestic heating is also necessary (as is shown in the continental case). However, a bare soil scheme can not correctly forecast the air temperatures in the canyon, and thus heat island intensities. Moreover, small-scale studies around an urbanized area do need a dedicated town model. The limit of the bare soil substitution is reached when purely urban areas are resolved in the atmospheric model. The TEB scheme is primarily aimed to these horizontal resolutions (from a couple hundred metres to tens of kilometres).

4.2. CONTINENTAL COLD CLIMATE: THE VALDAI CASE

Extreme continental meteorological conditions are now considered, with very cold winters, significant snow falls, and relatively warm summers. A large number of people are affected by such weather, because such climates are typical of metropoles in Canada, the U.S.A. and Asia. Domestic heating is known to play an important role in the urban energy budget for such conditions, and the ability of the TEB scheme to estimate this flux is now investigated. Furthermore, the importance of conduction through the surfaces allows the testing of, in a better way than with the oceanic forcing, the sensitivity of the scheme to the buildings' internal temperature and to the wall and roof structures.

The same qualitative characteristics about the energy flux evolution and repartition are found for urban diurnal cycles as in the Hapex-Mobilhy case. The focus of this study is on the annual cycle (Figure 13). The disparity between summer and winter is enhanced as compared to the previous case, especially with respect to the energy forcing: net radiation and building heat release. During winter, if buildings are built with the same material and insulation as in the oceanic region, the heat release from the buildings is as high as 150 W m^{-2} averaged for the month, all of this being transformed into sensible heat flux towards the atmosphere. The main part of this energy loss occurs through the walls, because the snow mantel of several tens of centimetres on the roofs acts as a supplementary insulation layer. The presence of snow explains the nearly zero latent heat flux during winter. The amount of energy necessary to melt it is shown by the thin solid line in Figure 13. Melting of the roof snow occurs (in this case) one month before the total disappearance of snow as observed in the countryside (not shown).

A sensitivity experiment on the insulation characteristics of the TEB scheme has been performed to test its response to the extremely cold weather conditions in winter. First, the internal wall and roof insulation layer was set four times thicker than the default value ('insulated' experiment). The internal building temperature is also allowed to vary down to 283.15 K (10 °C) in winter ('insulated, Ti' experiment). It is seen that the TEB formulation for the heating flux (prescribed internal temperature) is mainly sensitive to the wall and roof structure, and less to the internal temperature. Moreover, high building experiments (not shown) produce values up to 200 W m^{-2} or 250 W m^{-2} (insulated walls or not) for these fluxes in

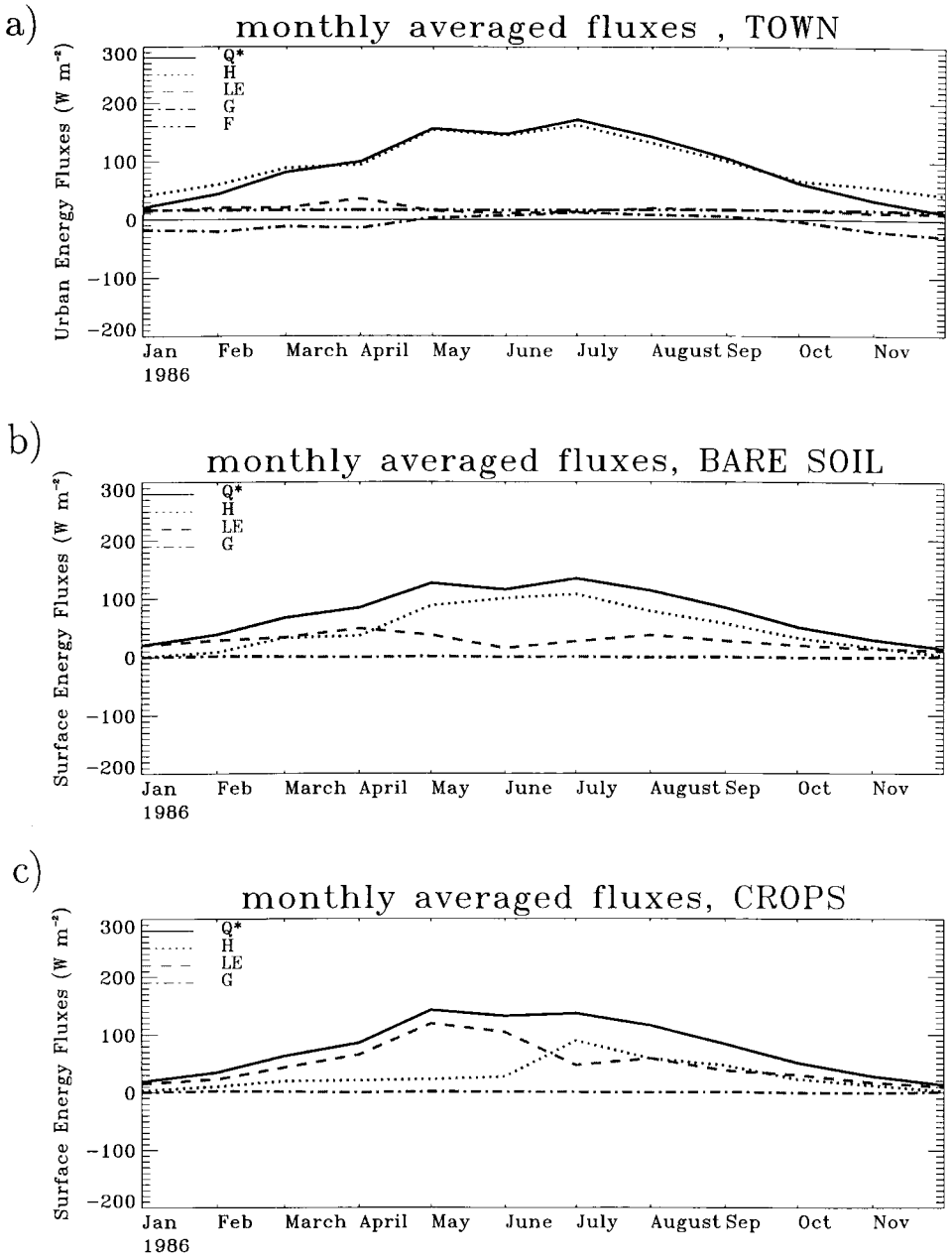

Figure 12. HAPEX-MOBILHY case: monthly averaged energy budget for three landscape types: (a) medium size city (reference simulation); (b) bare soil (20 cm deep); (c) crops. Same line convention as in Figure 8.

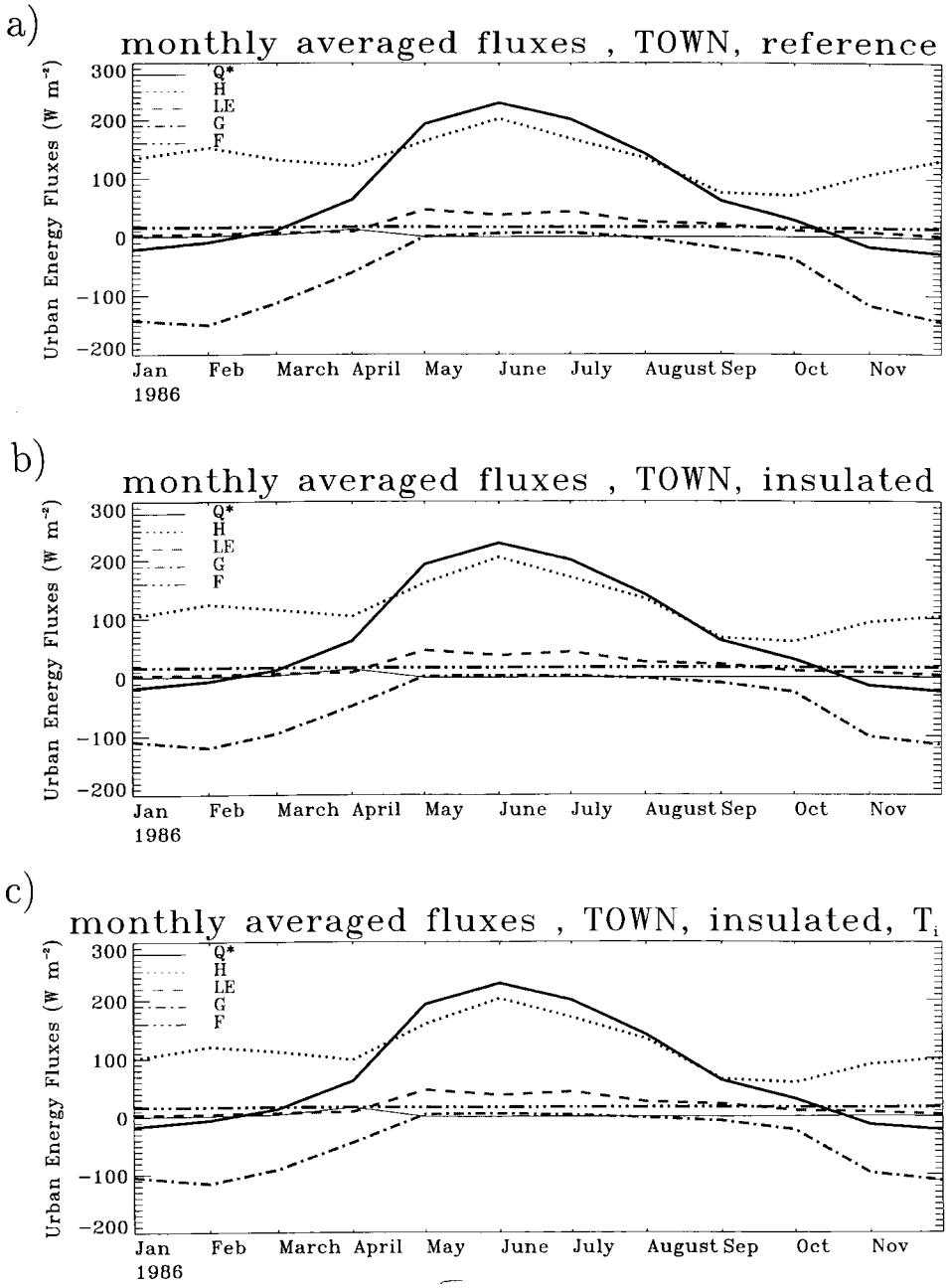

Figure 13. VALDAI case: monthly averaged energy budget for three city construction materials: (a) medium size city (reference simulation); (b) insulation increased (see Table III); (c) insulation increased, and internal building temperature varies from 283.15 K (10 °C) (winter) to 290.15 K (17 °C) (summer). Same line convention as in Figure 8. The thin solid line corresponds to the amount of energy necessary for melting.

winter. The building height is then a key parameter, not only for radiative trapping, but mostly for the conduction and surface turbulent flux exchange.

These very large fluxes seem realistic. Estimates of anthropogenic fluxes exist for some high latitude cities (Oke, 1988); for example, a value typical for Montreal ranges from 153 W m^{-2} in winter to 57 W m^{-2} in summer. The component dedicated to domestic heating can then be of the order of 100 W m^{-2} in winter; Moscow and Manhattan annual anthropogenic fluxes can be even 25 and 50% larger respectively.

5. Conclusion

The TEB surface scheme has been developed from various elements corresponding to the state of the art in urban climatology, and is aimed at representing the energy exchanges between cities and the atmosphere in a prognostic way. A simplification of the real city geometry was necessary. To our knowledge, this is the first time that the well-known canyon geometry is used to represent a city as part of the surface of an atmospheric model. An additional hypothesis of isotropy for the street directions has been added, in order to be representative of a city *quartier* (as defined in Mestayer and Anquetin, 1995). This allows the use of the scheme at horizontal scales larger than the road width, for local to regional impact studies. This also has the advantage that the scheme can be simplified to three surface energy budgets: one each for the roofs, the roads and the walls. The TEB model is then relatively easy to include in an atmospheric model, because only a few averaged parameters are needed, and the number of prognostic variables is comparable to that present in vegetation schemes for atmospheric models (see Tables I and II).

This relatively simple description of the town geometry is compensated by a complete physical package, as detailed in Sections 3 and 4. All weather conditions can be treated, day or night, and even precipitation events, without any ad-hoc assumption or tuning of the parameters. The radiative trapping is the subject of an original development, and is validated by comparison with specific measurements. One can then *be confident in the radiative energy inputs*. The sensitivity experiments showed that:

- the partition and diurnal hysteresis between the turbulent sensible heat fluxes and ground fluxes are correctly recovered by the scheme.
- the heat storage during the day can be greater than the turbulent heat flux. This effect is enhanced by high buildings.
- the latent heat can be neglected on average at the monthly time scale, but is very important when relatively short (daily) time scales are considered.
- the energy input from the building heat release can exceed the net radiation, especially in winter in continental climates. The model outputs are comparable to the few available estimates of city heat release.

The suburban experiment showed that the classical bare soil formulation used to represent cities in atmospheric models is good enough to represent the fluxes for large temporal or spatial averages; therefore, climatic or large-scale atmospheric models may not need an urban scheme at the present time. The prescription of the anthropogenic heat release still remains a problem. In contrast, town meteorological forecasts and mesoscale regional and local studies need such a scheme, as intensively urbanized energetics are very specific. An atmospheric model, coupled both to an aerosol radiatively active atmosphere (to have the correct radiative downward fluxes) and an urban surface scheme (to correctly distribute these fluxes), is necessary.

Long term in-situ measurements needed to validate an urban surface scheme are lacking. However, the TEB model behaves correctly compared to what is currently known from urban climatology. The next step will be the study of urban induced mesoscale flows, as validation data exist for typical situations (mainly heat-island episodes). This work is under way.

Acknowledgements

The author would like to thank Dr. J. Noilhan for his continuous help, and Dr. P. Bougeault and A. Boone for assistance in the preparation of the manuscript.

Appendix A: Solar Radiation Reflections

Suppose hereafter that the direct and scattered albedos for each surface are identical. If this is not the case, only the first direct solar reflection would be modified.

When the first reflection occurs, the fluxes stored by the road and wall, A_r and A_w, are respectively:

$$A_r(0) = (1 - \alpha_r)(S_r^{\Downarrow} + S_r^{\downarrow}),$$

$$A_w(0) = (1 - \alpha_w)(S_w^{\Downarrow} + S_w^{\downarrow}).$$

The reflected parts R_r and R_w are:

$$R_r(0) = \alpha_r(S_r^{\Downarrow} + S_r^{\downarrow}),$$

$$R_w(0) = \alpha_w(S_w^{\Downarrow} + S_w^{\downarrow}).$$

After n reflections:

$$A_r(n+1) = A_r(n) + (1 - \alpha_r)(1 - \Psi_r)R_w(n).$$

$$A_w(n+1) = A_w(n) + (1-\alpha_w)\Psi_w R_r(n) + (1-\alpha_w)(1-2\Psi_w)R_w(n),$$

$$R_r(n+1) = +\alpha_r(1-\Psi_r)R_w(n),$$

$$R_w(n+1) = +\alpha_w\Psi_w R_r(n) + \alpha_w(1-2\Psi_w)R_w(n).$$

Then,

$$A_r(n+1) = A_r(0) + (1-\Psi_r)(1-\alpha_r)\sum_{k=0}^{n} R_w(k),$$

$$A_w(n+1) = A_w(0) + \Psi_w(1-\alpha_w)\sum_{k=0}^{n} R_r(k),$$

$$+ (1-2\Psi_w)(1-\alpha_w)\sum_{k=0}^{n} R_w(k),$$

and

$$\sum_{k=0}^{n} R_r(k) = (1-\Psi_r)\alpha_r\sum_{k=0}^{n-1} R_w(k) + R_r(0),$$

$$\sum_{k=0}^{n} R_w(k) = \Psi_w\alpha_w\sum_{k=0}^{n-1} R_r(k) + (1-2\Psi_w)\alpha_w\sum_{k=0}^{n-1} R_w(k) + R_w(0).$$

Solving this geometric system yields, in the case of an infinite number of reflections,

$$\sum_{k=0}^{\infty} R_r(k) = \frac{R_r(0) + (1-\Psi_r)\alpha_r(R_w(0) + \Psi_w\alpha_w R_r(0))}{1-(1-2\Psi_w)\alpha_w + (1-\Psi_r)\Psi_w\alpha_r\alpha_w} = M_r,$$

$$\sum_{k=0}^{\infty} R_w(k) = \frac{R_w(0) + \Psi_w\alpha_w R_r(0)}{1-(1-2\Psi_w)\alpha_w + (1-\Psi_r)\Psi_w\alpha_r\alpha_w} = M_w.$$

The total solar radiation stored by road and wall is then:

$$S_r^* = (1-\alpha_r)S_r^{\Downarrow} + (1-\alpha_r)S_r^{\downarrow} + (1-\alpha_r)(1-\Psi_r)M_w,$$

$$S_w^* = (1-\alpha_w)S_w^{\Downarrow} + (1-\alpha_w)S_w^{\downarrow} + (1-\alpha_w)(1-2\Psi_w)M_w + (1-\alpha_w)\Psi_w M_r.$$

References

Aida, M.: 1982, 'Urban Albedo as a Function of the Urban Structure – A Model Experiment (Part I)', *Boundary-Layer Meteorol.* **23**, 405–413.

André, J., Goutorbe, J., Perrier, A., Becker, F., Bessemoulin, P., Bougeault, P., Brunet, Y., Brutsaert, W., Carlson, T., Cuenca, R., Gash, J., Gelpe, J., Hildebrand, P., Lagouarde, J., Lloyd, C., Mahrt, L., Mascart, P., Mazaudier, C., Noilhan, J., Ottlé, C., Payen, M., Phulpin, T., Stull, R., Shuttleworth, J., Schmugge, T., Taconet, O., Tarrieu, C., Thépenier, R., Valencogne, C., Vidal-Madjar, D., and Weill, A.: 1988, 'Evaporation over Land Surfaces: First Results from HAPEX-MOBILHY Special Observing Period', *Ann. Geophys.* **6**, 477–492.

Arnfield, J., Herbert, J. M., and Johnson, G. T.: 1998, 'A Numerical Simulation Investigation of Urban Canyon Energy Budget Variations', in *Proceedings of 2nd AMS Urban Environment Symposium*.

Arya, S. P.: 1988, *Introduction to Micrometeorology*, Academic Press, Inc., New York, 303 pp.

Best, M. J.: 1998, 'Representing Urban Areas in Numerical Weather Prediction Models', in *Proceedings of 2nd AMS Urban Environment Symposium.*

Bottema, M.: 1997, 'Urban Roughness Modelling in Relation to Pollutant Dispersion', *Atmos. Environ.* **18**, 3059–3075.

Deardorff, J.: 1978, 'Efficient Prediction of Ground Temperature and Moisture with Inclusion of a Layer of Vegetation', *J. Geophys. Res.* **83**, 1889–1903.

Feigenwinter, C., Vogt, R., and Parlow, E.: 1999, 'Vertical Structure of Selected Turbulence Characteristics above an Urban Canopy', *Theor. Appl. Climatol.* **62**, 51–63.

Grimmond, C. and Oke, T.: 1999a, 'Heat Storage in Urban Areas: Local-Scale Observations and Evaluation of a Simple Model', *J. Appl. Meteorol.* **38**, 922–940.

Grimmond, C. and Oke, T.: 1999b, 'Aerodynamic Properties of Urban Areas Derived from Analysis of Surface Form', *J. Appl. Meteorol.* **38**, 1262–1292.

Grimmond, C. S. B., Cleugh, H. A., and Oke, T. R.: 1991, 'An Objective Urban Heat Storage Model and its Comparison with Other Schemes', *Atmos. Environ.* **25B**, 311–326.

Grimmond, C. S. B. and Oke, T. R.: 1991, 'An Evapotranspiration-Interception Model for Urban Areas', *Water Resour. Res.* **27**, 1739–1755.

Grimmond, C. S. B. and Oke, T. R.: 1995, 'Comparison of Heat Fluxes from Summertime Observations in the Suburbs of Four North American Cities', *J. Appl. Meteorol.* **34**, 873–889.

Johnson, G. T., Oke, T. R., Lyons, T. J., Steyn, D. G., Watson, I. D., and Voogt, J. A.: 1991, 'Simulation of Surface Urban Heat Islands under 'Ideal' Conditions at Night. Part I: Theory and Tests Against Field Data', *Boundary-Layer Meteorol.* **56**, 275–294.

Mascart, P., Noilhan, J., and Giordani, H.: 1995, 'A Modified Parameterization of Flux-Profile Relationship in the Surface Layer Using Different Roughness Length Values for Heat and Momentum', *Boundary-Layer Meteorol.* **72**, 331–344.

Menut, L.: 1997, *Etude expérimentale et théorique de la couche limite Atmosphérique en agglomération Parisienne (Experimental and Theoretical Study of the ABL in Paris Area)*, Ph.D. Thesis, University Pierre et Marie Curie, Paris, France, 200 pp.

Mestayer, P.G. and Anquetin, S.: 1995, 'Climatology of Cities', in F.-S. Rys and A. Gyr (eds.), *Diffusion and Transport of Pollutants in Atmospheric Meso-Scale Flow Fields*, Atmospheric Sciences Library, Kluwer Academic Publishers, Dordrecht, pp. 165–189.

Mills, G. M.: 1993, 'Simulation of the Energy Budget of an Urban Canyon-I. Model Structure and Sensitivity Test', *Atmos. Environ.* **27B**, 157–170.

Noilhan, J.: 1981, 'A Model for the Net Total Radiation Flux at the Surfaces of a Building', *Building Environ.* **16**, 259–266.

Noilhan, J. and Planton, S.: 1989, 'A Simple Parameterization of Land Surface Processes for Meteorological Models', *Mon. Wea. Rev.* **117**, 536–549.

Nunez, M. and T. R. Oke: 1976, 'Long-Wave Radiative Flux Divergence and Nocturnal Cooling of the Urban Atmosphere. II: Within an Urban Canyon', *Boundary-Layer Meteorol.* **10**, 121–135.

Nunez, M. and Oke, T. R.: 1977, 'The Energy Balance of an Urban Canyon', *J. Appl. Meteorol.* **16**, 11–19.

Oke, T. R.: 1987, *Boundary Layer Climates*, 2nd edn., Methuen, London, 435 pp.

Oke, T. R.: 1988, 'The Urban Energy Balance', *Prog. Phys. Geogr.* **12**, 471–508.

Oke, T., Spronken-Smith, R., Jáuregui, E., and Grimmond, C.: 1999, 'The Energy Balance of Central Mexico City during the Dry Season', *Atmos. Environ.* **33**, 3919–3930.

Petersen, R. L.: 1997, 'A Wind Tunnel Evaluation of Methods for Estimating Surface Roughness Length at Industrial Facilities', *Atmos. Environ.* **31**, 45–57.

Richards, K. and Oke, T. R.: 1998, 'Dew in Urban Environments', in *Proceedings of 2nd AMS Urban Environment Symposium*.

Ross, S. L. and Oke, T. R.: 1988, 'Tests of Three Urban Energy Balance Models', *Boundary-Layer Meteorol.* **44**, 73–96.

Rotach, M. W.: 1995, 'Profiles of Turbulence Statistics in and above an Urban Street Canyon', *Atmos. Environ.* **29**, 1473–1486.

Roth, M.: 1993, 'Turbulent Transfert: Relationships over an Urban Surface. II: Integral Statistics', *Quart. J. Roy. Meteorol. Soc.* **119**, 1105–1120.

Roth, M. and Oke, T.: 1993, 'Turbulent Transfert: Relationships over an Urban Surface. II: Spectral Characteristics', *Quart. J. Roy. Meteorol. Soc.* **119**, 1071–1104.

Rowley, F.B., Algren, A. B., and Blackshaw, J. L.: 1930, 'Surface Conductances as Affected by Air Velocity, Temperature and Character of Surface', *ASHRAE Trans.* **36**, 429–446.

Rowley, F. B. and Eckley, W. A.: 1932, 'Surface Coefficients as Affected by Wind Direction', *ASHRAE Trans.* **38**, 33–46.

Schlosser, C.A., Robock, A., Vinnikov, K., Speranskaya, N., and Xue, Y.: 1997, '18-Year Land Surface Hydrology Model Simulations for a Midlatitude Grassland Catchment in Valdai, Russia', *Mon. Wea. Rev.* **125**, 3279–3296.

Seaman, N. L., Ludwig, F. F., Donall, E. G., Warner, T. T., and Bhumralkar, C. M.: 1989, 'Numerical Studies of Urban Planetary Boundary-Layer Structure under Realistic Synoptic Conditions', *J. Appl. Meteorol.* **28**, 760–781.

Soux, A., Oke, T. R., and Voogt, J. A.: 1998, 'Modelling and Remote Sensing of the Urban Surface', in *Proceedings of 2nd AMS Urban Environment Symposium*.

Sturrock, N. and Cole, R.: 1977, 'The Convective Heat Exchange at the External Surface of Buildings', *Building Environ.* **12**, 207–214.

Taha, H.: 1999, 'Modifying a Mesoscale Meteorological Model to Better Incorporate Urban Heat Storage: A Bulk-Parameterization Approach', *J. Appl. Meteorol.* **38**, 466–473.

Terjung, W. H. and O'Rourke, P. A.: 1980, 'Influences of Physical Structures on Urban Energy Budgets', *Boundary-Layer Meteorol.* **19**, 421–439.

Wieringa, J.: 1993, 'Representative Roughness Parameters for Homogeneous Terrain', *Boundary-Layer Meteorol.* **63**, 323–363.